Analysis of defense-related gene expression and leaf metabolome in wheat during the early infection stages of Blumeria graminis f.sp. tritici

Thierry Allario, Alice Fourquez, Maryline Magnin-Robert, Ali Siah, Matthieu Gaucher, Alessandra Maia-Grondard, Marie-Noelle Brisset, Philippe Hugueney, Philippe Reignault, Raymonde Baltenweck, et al.

Analysis of defense-related gene expression and leaf metabolome in wheat during the early infection stages of *Blumeria graminis* f.sp. *tritici*

Thierry Allario, [1*] Alice Fourquez, [1*] Maryline Magnin-Robert, [1] Ali Siah, [2] Alessandra Maia-Grondard, [4] Matthieu Gaucher, [3] Marie-Noelle Brisset, [3] Philippe Hugueney, [4] Philippe Reignault, [1] Raymonde Baltenweck, [4* §], Beatrice Randoux [1* §]

[(1)] Univ. Littoral Côte d'Opale, Unité de Chimie Environnementale et Interactions sur le Vivant (UCEIV-UR 4492), SFR Condorcet FR CNRS 3417, CS 80699, F-62228, Calais cedex, France.

[(2)] Joint Research Unit 1158 BioEcoAgro, Junia, Univ. Lille, Univ. Liège, UPJV, ULCO, Univ. Artois, INRAE, 2 Rue Norbert Ségard, F-59014, Lille, France.

[(3)] IRHS-UMR1345, Université d'Angers, INRAE, Institut Agro, SFR 4207 QuaSaV, F-49071,
42 rue Georges Morel, F-49071 Beaucouzé cedex, France.

[(4)] Université de Strasbourg, INRAE, SVQV UMR-A 1131, F-68000 Colmar, France.

[*] These authors contributed equally to this work

[§] Corresponding authors: Beatrice Randoux; E-mail: Beatrice.Randoux@univ-littoral.fr; Raymonde Baltenweck; E-mail: raymonde.baltenweck@inrae.fr

Keywords: Wheat – RT-qPCR – Metabolomic – Powdery mildew – Plant defense– Hydroxycinnamic acid amides – Pipecolic acid – Phenylpropanoid pathway

Funding: This research was conducted in the framework of the project CPER Alibiotech, funded by the European Union, the French State, the French Region Hauts de France and ULCO.

ABSTRACT

Blumeria graminis f.sp. *tritici* (*Bgt*) is an obligate biotrophic fungal pathogen responsible for powdery mildew in bread wheat (*Triticum aestivum L.*). Upon *Bgt* infection, the wheat plant activates basal defense mechanisms namely PAMP-triggered immunity (PTI) in the leaves during the first few days. Understanding this early stage of quantitative resistance is crucial for developing new breeding tools and evaluating plant resistance inducers for sustainable agricultural practices. In this sense, we used a combination of transcriptomic and metabolomic approaches to analyze the early steps of the interaction between *Bgt* and the moderately susceptible wheat cultivar Pakito. *Bgt* infection resulted in an increasing expression of genes encoding pathogenesis-related proteins (PR-proteins, *PR1*, *PR4*, *PR5* and *PR8*), known to target the pathogen, during the first 48 hours post-inoculation. Moreover, RT-qPCR and metabolomic analyses pointed out the importance of the phenylpropanoid pathway in quantitative resistance against *Bgt*. Among metabolites linked to this pathway, hydroxycinnamic acid amides containing agmatine and putrescine as amine component accumulated from the second to the fourth day after inoculation. This suggests their involvement in quantitative resistance *via* cross-linking processes in cell wall for reinforcement, what is supported by the up-regulation of *PAL* (phenylalanine ammonia-lyase), *PR15* (encoding an oxalate oxidase) and *POX* (peroxidase) after inoculation. Finally, pipecolic acid, which is considered as a signal involved in systemic

acquired resistance (SAR), accumulated after inoculation. These new insights lead to a better understanding of basal defense in wheat leaves after *Bgt* infection.

INTRODUCTION

Bread wheat (*Triticum aestivum L.*) is the most widespread staple food for humans with a constant increasing demand due to the growing human population (FAO, 2018). This major food crop is constantly threatened by attacks from diverse foliar fungi, and particularly the biotrophic ascomycete fungus *Blumeria graminis f. sp. tritici* (*Bgt*) causing the powdery mildew disease. Powdery mildew is widely dispersed in temperate and humid regions of the world and provokes powdery white sporulating colonies emerging on wheat leaves and stems. This foliar disease affects wheat grain quality and can lead to severe yield losses up to 34% (Gao et al., 2018), and particularly when the fungus affects the ears. Plants suffer as a result of the rerouting of nutrients into the fungus (Mwale et al., 2014; Gao et al. 2018). This fungus overwinters mainly on plant debris with ascospores produced by sexual reproduction, which serve as primary inoculum in favorable environmental conditions. New fungal infections are produced by wind-dispersed spores blowing onto uninfected plants, and successive asexual reproduction cycles are responsible for the disease spreading. The generation time (time from spore germination to spore production) of the powdery mildew fungus can be as short as 7 to 10 days and a large number of spores may be produced each asexual generation. The infection process begins when spores germinate and form first a primary germ tube. Then a second germ tube, called

appressorial germ tube, emerges from the spore and forms the appressorium which enters the epidermal cell wall and generates a feeding structure called haustorium by invagination of the plasmalemma. The haustorial plasma membrane establishes a very close interface with the host plasma membrane and extracellular matrix to absorb plant host nutrients (Mwale et al., 2014; Gao et al., 2018). Mycelium develops on leaf surface and new appressoria and haustoria are formed. Asexual spores are then produced again and are rapidly dispersed by wind to infect other wheat plants.

Because the use of fungicides is not environmentally friendly, cultivation of resistant cultivars appears to be the most effective, economical, and environmentally safe approach to control powdery mildew disease (Gao et al., 2018). The ability of host plants to impede a given microbial pathogen to colonize its tissues determine the degree of susceptibility of the plant to this pathogen (Dangl and Jones, 2001; Jones and Dangl, 2006). To counterattack pathogen infection, plants have developed the ability to sense pathogens and to initiate immune responses. In the case of a biotrophic pathogen, such as *Bgt*, two interconnected defense lines leading to plant immunity have been depicted with namely, the pathogen-associated molecular pattern-triggered immunity (PTI) and the effector-triggered immunity (ETI). First, molecular structure of constitutive compounds of pathogen cell wall, such as chitin and glucans during a plant-pathogenic fungus interaction, can be recognized by the plant cell as pathogen-associated molecular patterns (PAMPs), thanks to transmembrane pattern recognition receptors (PRRs). After recognition, the PAMP-Triggered Immunity (PTI), also known as basal resistance, is activated to impede pathogen proliferation (Nürnberger et al., 2004; Zipfel and Felix, 2005). Nevertheless, successful pathogens are able to produce effectors disrupting PTI and strengthening pathogen virulence, which results in

effector-triggered susceptibility (ETS; Jones and Dangl, 2006). For instance, the RNase-like effector CSEP0064/BEC1054 produced by *Bgt* has recently been proposed to inhibit the plant ribosome-inactivating proteins (RIPs) which, otherwise, could lead to host cell death at the infection site and could prevent the colonization of wheat by pathogen fungi (Pennington et al., 2019). Nevertheless, effectors secreted by the pathogen can in turn be identified by a specialized group of plant resistance (R) proteins that induce the effector-triggered immunity (ETI) mobilizing highly efficient plant defense reactions. Plant breeders have mostly developed a breeding strategy conferring a race-specific resistance through hypersensitive reactions (Huang and Röder, 2004, Chen et al., 2005), corresponding to ETI expression. In wheat, up to now, 88 powdery mildew resistance (Pm) genes or alleles have been identified (McIntosh et al., 2019; Li et al., 2020; Zhu et al., 2020). However, this kind of qualitative resistance is frequently overcome with the emergence of new races of fungus presenting the corresponding virulence genes (Miedaner et al., 1993; Zhu et al., 2020). Another breeding strategy in wheat, which is race-nonspecific and known as “slow-mildewing” or “partial resistance”, consists to play on a set of factors leading to slow down the disease progress and allow the plant to mature before the manifestation of damaging symptoms (Piarulli et al., 2012). Indeed, principal differences between PTI and ETI are quantitative and/or temporal rather than qualitative, engaging plants and microbial pathogens in a race-to-survive which determine plant resistance or plant susceptibility (Yuan et al., 2021; Katagiri et al., 2004). Moreover, new control strategies of plant diseases are currently explored to bring about new control means meeting the requirements of efficacy and environmental protection. Exogenous application of elicitors can result in an induced resistance in susceptible cultivars, *via* direct induction or priming of plant defenses able to impede or limit a specific step of the fungus

infectious process (Walters et al., 2013). Understanding basal defense associated with PTI is then crucial to select effective elicitors leading to plant protection. In this sense, exploring the plant responses during a compatible interaction between a moderately susceptible cultivar and an infectious strain of *Bgt* may highlight pathways that could be triggered for induced resistance.

In this study, we combined a transcripts analysis with targeted and untargeted metabolomic analysis in order to better characterize the compatible interaction between *Bgt* and a moderately susceptible cultivar of *Triticum aestivum* L (cv. Pakito). We used a biomolecular RT-qPCR based low-density microarray tool to analyze the expression of 26 genes, considered as molecular markers of the main defense mechanisms, such as genes encoding PR proteins, genes involved in phenylpropanoid pathway, isoprenoid pathway, antioxidant system, synthesis of parietal compounds for reinforcement of cell walls or others signaling pathways (Brisset et Dugé de Bernonville, 2011; Dugé de Bernonville et al., 2014). In parallel, targeted and untargeted metabolomic analysis using ultra-high-performance liquid chromatography coupled to high resolution mass spectrometry highlighted major changes in wheat leaf metabolome in response to *Bgt* infection, which could be linked with the induction of specific defense-related genes.

MATERIALS AND METHODS

Biological material and growth conditions

Bread wheat (*Triticum aestivum* L.) cv. Pakito, which was provided by RAGT (Rodez, France), is susceptible to the MPEBgt1 powdery mildew isolate of *Blumeria graminis* f. sp. *tritici* (*Bgt*) (Tayeh et al., 2015; Mustafa et al., 2017). Twenty four wheat grains were soaked overnight in water, then grown into trays containing compost (600 g Terreau Floradur A 70L, Ref 16311470) and transferred in culture chambers (Panasonic, MLR-352H) with a relative humidity of 70%, a photoperiod of 12h/12h, a luminous intensity of 250 $\mu mol.m^{-2}.s^{-1}$, a day temperature of 18°C and a night temperature of 12°C (Randoux et al., 2006).

The fungus was inoculated and maintained on cv. Alixan (Limagrain, Vertaizon, France) in a separate chamber (Randoux et al., 2006). Following a method previously established by Randoux et al. (2006), heavily sporulating leaves were shaken above 11-day old plants in order to obtain fresh sporulating leaves after 10 days for the fungal inoculations in this study.

Inoculation of wheat plants

Twelve-day-old wheat plantlets were inoculated with 5 mL of a suspension of *Bgt* spores (500 000 spores/mL in Fluorinert FC43, heptacosafluorotributhylamine 3M, Cergy-Pontoise, France) with a sprayer (ITW Surfaces et Finitions, Valence, France). Mock-infected plants were sprayed with 5 mL of Fluorinert FC43 (heptacosafluorotributhylamine 3M, Cergy-Pontoise, France). Twelve days after inoculation, the symptoms were checked through the development of white colonies on the first leaf, what confirms the successful infection of plantlets by *Bgt*.

RNA extraction and real-time quantitative reverse-transcription polymerase chain reaction analysis of gene expression

Samplings for the analysis of defense gene expression were carried out on the first leaves of seedlings, 24 and 48 hours post-inoculation (hpi) by *Bgt* and corresponding control plants. Sampled leaves were frozen in liquid N and stored at -80°C before use. Total RNA was extracted from 100 mg of grounded leaf tissues using the QIAGEN RNeasy mini kit (Qiagen, Hilden, Germany) following the manufacturer's instructions with few modifications concerning 5 additional steps of washing with RPE buffer (Qiagen, Hilden, Germany). Genomic DNA contaminating the samples was removed by treatment with the RNAse-Free DNase Set (Qiagen, Hilden, Germany). RNA was eluted with 50 µl of RNase Free water (Qiagen, Hilden, Germany). RNA quality was checked by running all RNA extracts on TAE Agarose gel 1% and RNA quantification was performed by measuring the absorbance at 260 nm using a biophotometer (Eppendorf, Hambourg, Germany). In total, 1 µg of total RNA was reverse-transcribed using the High Capacity cDNA Reverse Transcription Kit (Thermofisher scientific – ancient ref. Applied Biosystems, Foster City, CA, USA) following the manufacturer's protocol. The expression level of wheat targeted genes was assessed by quantitative PCR using the bio-molecular tool patended by Brisset and Dugé de Bernonville (2011). The tool allows the simultaneous quantification of expression of 26 genes that represent a wide diversity of very well-known defense mechanisms in plants i.e. PR proteins, secondary metabolism, oxidative stress, cell-wall modification, salicylic acid (SA)/jasmonic acid (JA)/ethylene (ET) signaling pathways. Reactions were carried on a Biorad CFX connect (Biorad, Hercules, CA, USA) using the SYBR SsoAdvanced Universal Green Supermix (Biorad, Hercules, CA, USA) according to the

manufacturer's protocol and the following thermal profile: 15 s at 95°C (denaturation) and 1 min at 60°C (annealing/extension) for 40 cycles. Melting curve assay was performed from 65 to 95°C at 0.5°C/s. Melting peaks were visualized for checking the specificity of each amplification. The real time PCR analysis concerns twenty-six genes associated to several wheat defense mechanisms as listed in Table 1. *Tubβ*, *GADPH* and *Actin* were used as internal reference genes for normalization. The results represent the relative expression in leaf tissues of pathogen-inoculated plants (I) versus those corresponding to control (NI) according to the $2^{(-\Delta\Delta Ct)}$ method described by Schmittgen and Livak (2008) and expressed in log2 fold change. Values of gene expression level are the average of gene expressions of three distinct plants (biological replicates) for which three gene expression analysis per plant were made for each gene studied (technical replicates). Two independent experiments (Exp.1 and Exp.2) were realized to confirm the results.

Targeted metabolomic analysis

Sampling of infected (I) and mock-infected (NI = non-infected) plants was performed 24, 48, 72- and 96-hours post-inoculation (hpi), using nine biological replicates for each condition and time point. Leaves were collected, frozen into liquid nitrogen and stored at -80°C until analysis. Leaves were freeze-dried for 24 hours (Freezone 2.5, Labconco, Kansas City, USA) and each sample was weighed (dry weights were between 20 and 25 mg). Leaves were then transferred into 2 mL Eppendorf tubes and 2 stainless steel beads (3.2 mm diameter, Dutscher, Brumath, France) were added. The leaves were crushed 4 times during 30 s at a speed of 30 movements/s in a bead mill (TissueLyser II, Qiagen, Venlo, Netherlands) to obtain a powder. Metabolites were

extracted with methanol (25 µL/mg dry weight) supplemented with 1 µg.mL^{-1} apigenin and 5 µg.mL^{-1} chloramphenicol (Sigma-Aldrich) as internal standards. The samples were sonicated in an ultrasonic bath (FB15050, Fisher Scientific, Hampton, USA) for 10 min and centrifugated at 12000 g for 15 min. Supernatants were analyzed by ultra-high-performance liquid chromatography coupled to high resolution mass spectrometry (UHPLC-HRMS) as described previously (de Borba et al., 2021). Metabolites belonging to different chemical families were identified based on published works about benzoxazinoids (de Bruijn et al., 2016), flavonoids (Wojakowska et al., 2013) and hydroxycinnamic acid amides (HCAAs) (Li et al., 2018) from wheat. Putative metabolite identifications were proposed based on expertized analysis of the corresponding mass spectra and comparison with published literature. Relative quantification of the selected metabolites was performed using the Xcalibur software (Thermo Fisher Scientific, Waltham, MA, USA). For some metabolites, identity was confirmed with the corresponding standard provided by Sigma-Aldrich (France). Differential metabolomic analyses were performed using the Tukey's Honest Significant Difference (HSD) method followed by a false discovery rate (FDR) correction using the Benjamini-Hochberg procedure (Benjamini and Hochberg, 1995). Metabolites of interest were considered differentially accumulated when the false discovery rate was below 5% (FDR < 0.05).

Non-targeted metabolomic analysis

For non-targeted metabolomic analysis, raw data were converted into mzXML format using MSConvert. mzXML data were organized into eight classes according to the infection status (NI/I) and hpi conditions plants. They were then processed using the

XCMS software package (Smith et al. 2006). Settings of XCMS were as follows: the method to extract and detect ions used was “centWave”, ppm (parts per million) = 3, noise = 30 000, mzdiff = 0.001 (mzdiff representing the minimum difference in m/z dimension required for peaks with overlapping retention times), prefilter = c (5,15000), which means that mass traces are only retained for the analyses if they contain at least 5 peaks with intensity >=15000, snthresh (defining the signal to noise ratio cutoff) = 6, peak width = c (5,35). Peaks were aligned using the obiwarp function using the following group density settings: bw (defining the bandwidth (standard deviation) to be used) = 10, mzwid (defining the width of overlapping m/z slices to use for creating peak density chromatograms and grouping peaks across samples) = 0.005, minimum fraction of samples for group validation: 0.5. Using these settings, 3140 ion identifiers were generated by XCMS script as MxxxTyyy, where xxx is the *m/z* ratio and yyy the retention time in seconds. For each ion identifier in each sample, relative quantitation data (peak area) were used for statistical analyzes. Differentially accumulated metabolites that discriminate I from NI plants were selected as follows: the "diffrepport" function of the XCMS software was used to perform a two-group Welch t-test for each ion. Ions significantly differentially accumulated were selected based on a p-value threshold < 0.05 and a fold change threshold ≥ 2. Comparison of I and NI leaves at 48 hpi, resulted in 81 differentially accumulated ions (Supp. Table 3), which were sorted by retention time (RT) in order to group ions potentially originating from the same molecule. Putative molecular formulas were proposed based on the precise mass of the ions, isotopic ratios, adducts and loss of neutrals, as well as by comparison with published literature.

RESULTS

Effect of *Bgt* infection on the expression of defense-related genes in leaf tissues

The relative expression level of 26 defense-related genes of wheat was monitored 24 and 48 hours post-inoculation (hpi) by *Bgt* spores of twelve-day-old plantlets. The functions of these genes are described in Supp Table 1. The average expression level of each gene was measured in inoculated plants (I-plants) compared to non-inoculated plants (NI-plants) and reported on a heatmap profile (Fig.1) for two independent experiments (Exp.1 and Exp.2). Genes with different patterns in their expression levels (i.e. no expression change, up-regulation and down-regulation) between the experiment 1 and the experiment 2 were not considered. Most of genes encoding PR-proteins were strongly induced during the first day after inoculation. Indeed, *PR1* (pathogenesis-related protein 1), *PR4* (pathogenesis-related protein 4 – hevein like protein) and *PR5* (pathogenesis-related protein 5 – thaumatin like protein) were strongly up-regulated 24 hpi and their expression were reinforced at 48 hpi by amount 11-, 9- and 9-fold in Exp.1, and by amount 9-, 8- and 8-fold in Exp.2, respectively. The level of *PR15* (pathogenesis-related protein 15 – oxalate oxidase) expression was slightly increased 24 hpi and also strengthened 48 hpi (3-fold), whereas the *PR8* (pathogenesis-related protein 8 – class I chitinase) was only induced 48 hpi. Concerning the genes encoding proteins involved in the phenylpropanoid pathway, the expression level of *PAL* (phenylalanine ammonia-lyase) appeared to be up-regulated at 24 and 48 hpi with a peak at 24 hpi reaching 6-fold in Exp.1 and 5-fold in Exp.2, respectively, while *FNS* (flavone synthase) and CHS (chalcone synthase) were not induced. *WRKY* (WRKY transcription factor 53), involved in the regulation of oxidative

responses to a wide array of stresses in wheat, was strongly up-regulated 24 hpi (6- and 5-fold in Exp.1 and Exp.2, respectively) and decreased to reach 3- and 2-fold the next day (Exp.1 and Exp.2, respectively). Regarding antioxidant systems, a strong and constant up-regulation of *POX* (peroxidase) across the two days (from 10-fold to 11-fold in Exp.1 and from 9-fold to 12-fold in Exp.2) accompanied with a slight up-regulation of *GST* (glutathione S-transferase), around 1.5-fold in both experiments, 48 hpi, were noticed. The expression profile of genes involved in isoprenoid pathway displayed a contrasted pattern. If *HMGR* (hydroxymethyl glutarate-CoA reductase) was up-regulated during the first day after inoculation and reduced the next day from 2-fold to 1.5-fold in Exp.1 and from 2-fold to 0.7-fold in Exp.2, no significant change of expression was noticed for *FPPS* (farnesyl pyrophosphate synthase) while *FAR* ((E,E)-alpha-farnese synthase) was gradually and strongly down-regulated over time. A limited effect of *Bgt* infection was detected on wheat genes of the ethylene signaling group. *ACCS* (1-aminocyclopropane-1-carboxylate synthase) was transiently and slightly down-regulated 24 hpi between NI-plants and I-plants while no change of expression was observed in *EIN3* (EIN3-binding F box protein 1) expression levels.

Overall, RT-qPCR analysis performed on wheat plants inoculated with *Bgt* has revealed specific patterns of defense gene expression. In each group of defense genes studied, specific genes were found upregulated, downregulated or unchanged over time. However, we can cluster each group following the change of gene expression level between 24 hpi and 48 hpi. The expression level of genes from parietal compounds group *CalS* (callose synthase), *CesA* (cellulose synthase A) and *CAD* (cinnamyl-alcohol dehydrogenase)), cystein sulfoxide group (*CSL* (cysteine sulfoxide)) and jasmonic acid signaling group (*JAR* (jasmonate resistant 1)) was unchanged between NI-plants and I-plants. All genes of the pathogenesis-related group that were

upregulated the first day after inoculation, i.e. *PR1*, *PR4*, *PR5*, *PR8* and *PR15*, had their expression level strengthened the next day contrasting the fact that all genes of the phenylpropanoid pathway group, the salicylic acid signaling group and the isoprenoid pathway group that were upregulated (*PAL*, *WRKY, HMGR*), or downregulated 24 hpi (*FAR*), had their gene expression level lowered 48 hpi. Finally, genes belonging to the antioxidant systems group were upregulated similarly during the two days (*POX*) or only upregulated the second day (*GST*).

Impact of *Bgt* inoculation on a selection of wheat leaf metabolites

Targeted metabolomic analysis using UHPLC-HRMS was undertaken to assess the impact of *Bgt* inoculation on the wheat leaf metabolome during a compatible interaction. The plant response was investigated 24, 48, 72 and 96 hours after inoculation by comparing leave extracts of infected plants to mock-infected ones. This targeted analysis allowed the detection and the relative quantification of 53 metabolites classified in 5 chemical or functional families: amino acids (AA), benzoxazinoids (BZ), flavonoids (F), phytohormones (H), and hydroxycinnamic acid amides (HCAAs) (Supplemental Table 2). Benzoxazinoids are plant defense metabolites found in many Poaceae species and are known to display antimicrobial and allelopathic activities (Hashimoto and Shudo, 1996; de Bruijn et al., 2018). Hydroxycinnamic acid amides are a family of plant secondary metabolites reported to be positively correlated with plant resistance in several pathosystems (Muroi et al., 2009; Gunnaiah et al., 2012; Yogendra et al., 2014). Phytohormones are particularly crucial in defense against pathogen attacks. Salicylic acid (SA) is considered to be the key hormone regulating defense against biotrophic pathogens, while jasmonic acid (JA) would trigger defense mechanisms toward necrotrophic invaders. Methyl salicylate (MeSA) is an essential

signal for establishing SAR (Thaler et al., 2012). In the wheat-*Bgt* pathosystem, salicylic acid (SA) and jasmonate (JA) signaling-related genes were differentially expressed, thus suggesting that they are involved in the defensive response against Bgt infection (Wang et al., 2012).

Infection with *Bgt* resulted in substantial differences in global wheat leaf metabolite patterns, as highlighted by a PCA analysis performed on all samples and all quantified metabolites, where the first and the second components explained 21.3%, 21,1% of the variances, respectively (Figure 2). Samples corresponding to (I) conditions are separated from mock-infected controls from 24 hpi on, along the second-dimension axis.

A differential analysis was then carried out in order to analyze the impact of *Bgt* infection on the accumulation of selected metabolites. For each time point, fold changes of significant differentially accumulated metabolites (DAMs) between I and NI conditions are presented as a heatmap (Fig. 3). During the first days after inoculation with *Bgt*, 11 of the 53 analyzed metabolites were differentially accumulated in *Bgt*-infected wheat leaves compared to control leaves (Fig. 3). DAMs included three amino acids (Phe, Glu and His), two amino acid derivatives (agmatine and pipecolic acid), and several HCAAs. Conversely, *Bgt* inoculation did not significantly impact the accumulation of the selected metabolites in the benzoxazinoid and flavonoid families. Looking in more details at the kinetic of wheat infection by *Bgt*, no DAM was detectable at 24 hpi. From 72 hpi, inoculation with *Bgt* impacted significantly but slightly the accumulation of phenylalanine, glutamine, histidine, and later (96 hpi), pipecolic acid (Fig. 3, Fig. 4). Finally, inoculation with *Bgt* resulted in a massive accumulation of HCAAs, some of them increasing by a factor 20 in *Bgt*-infected leaves compared to control leaves (Fig.3).

Untargeted metabolomic analyses of the wheat - *Bgt* interaction

As a complement to the quantification of a set of selected metabolites, untargeted metabolomic were used to further analyze the impact of *Bgt* infection on wheat leaf

metabolome. Combined analysis of raw mass spectrometry data of all samples revealed 3140 ions, which were further considered for differential analyses. Ions of interest were selected based on a statistically significant differential accumulation (p value < 0.05) between *Bgt*-infected and control wheat leaves at 48 hpi, with a fold change > 2. This selection process resulted in a set of 81 differentially accumulated ions (Supp Table 3), which were further investigated for tentative identification of some of the corresponding molecules. To this end, ions with similar retention times, potentially derived from the same molecules, were investigated for identification as pseudo-molecular ions, fragments and isotopes.

For example, the mass spectrum with peak identifier M291T255 (group 5) showed a pseudo-molecular ion *m/z* 291.1451 corresponding to the chemical formula $C_{14}H_{19}O_3N_4$ (Supplemental Figure 1). This ion was furthermore associated with a fragment *m/z* 273. 1346 ($C_{14}H_{17}O_2N_4$) corresponding to the loss of a water molecule from the molecular ion, and a fragment *m/z* 147.0440 corresponding to a coumaroyl moiety $C_9H_7O_2$. Combination of this spectral information made it possible to propose that M291T255 and the related ions were derived from coumaroyl-hydroxy-dehydro-agmatine (Supplemental Figure 1, Figure 6). This agmatine derivative has recently been identified in wheat leaves infected with *Bipolaris sorokiniana*, the causative agent of spot blotch of Poaceae (Ube et al., 2019a), and the corresponding hydroxylated agmatine, the *p*-coumaroyl-3-hydroxy-agmatine, has been characterized in wheat submitted to cold stress (Jin et al., 2003).

Taking advantage of the excellent accuracy of the mass measurements (< 1 ppm), in-depth analysis of high-resolution mass spectra made it possible to assign a plausible chemical formula and then a structural proposal for 16 of the 81 ions (Supp Table 3).

Most of the assigned chemical formulas corresponded to HCAAs. Some metabolites have been tentatively identified according to published literature and the PubChem database (https://pubchem.ncbi.nlm.nih.gov/). Analysis of differential accumulation of these 81 ions between I and NI conditions was performed at different time points (Figure 5). Most of these ions were not significantly differentially accumulated at 24 hpi, suggesting that the metabolic impact of *Bgt* infection starts to be significant after this time point. However, most ions accumulated further and with larger fold changes at 72 and 96 hpi, especially those associated to HCAAs (Figure 5, Supp Table 3).

DISCUSSION

In our study, we combined an analysis of defense related-gene expression and metabolite accumulation to provide an overview on the main mechanisms that occur during the first steps of powdery mildew infection in a moderately susceptible bread wheat cultivar. First, PR-protein genes were mainly up-regulated, which is consistent with the observations made in other studies (Liljeroth et al., 2001; Wu et al., 2014), depicting an accumulation of PR protein transcripts in both susceptible and resistant wheat in response to pathogen infection, but with a greater abundance of PR-proteins in the most resistant plants than in the susceptible ones (Geddes et al., 2008). Moreover, the accumulation of glutamine, histidine and phenylalanine suggests an elevated biosynthesis of amino-acids that would serve as building blocks for both PR-proteins and phenylpropanoids as described during a compatible interaction between barley and *Blumeria graminis* f. sp. *hordei* (Voll et al., 2011). In Pakito, PR1, PR4, PR5, PR8 and PR15 are involved in partial defense mechanisms taking place during the first two days after *Bgt* inoculation. PR4, also known as hevein-like proteins, and PR8, a class I chitinase, are both endochitinases able to disrupt fungal cell wall into small

components used as elicitors by the plant cell to mediate plant defense response (Shoresh and Harman, 2008). Hevein-like proteins are also able to inhibit the hyphal growth of fungi by binding to chitin and can have an antimicrobial activity in plants (Nawrot et al., 2014). Antifungal hevein-type peptides with high inhibitory activity have already been reported in *Triticum kiharae* seeds facing various pathogenic fungi and bacteria (Huang et al., 2002). According to our results, *PR4* is strongly up-regulated from the first 24 hours after *Bgt* inoculation whereas *PR8* expression increased 48 hours after inoculation. In the susceptible Orvantis wheat cultivar, the up-regulation of some chitinase-encoding genes occurred between 9 and 21 hpi and was correlated to the developmental stage of *Bgt* leading from conidia with primary germ tube to conidia with appressorial germ tube. This up-regulation of chitinase-encoding genes was followed with an increasing activity of chitinase enzymes 24 hpi, suggesting their role in degrading chitin polymers from the fungal pathogen cell wall at the time of the appressorial germ tube penetration (Tayeh et al., 2015).

Two other PR-proteins, *PR1* and *PR5,* exhibited the same expression patterns than *PR4* with a strong up-regulation 24 hpi strengthened 48 hpi. They code respectively a protein with antimicrobial properties, known to be expressed in association with SAR, and a thaumatin-like protein, known to have antifungal activities targeting pathogenic fungi hyphae and spores (Niderman et al., 1995; Singh et al., 2014; Enoki and Suzuki 2016).

Moreover, pipecolic acid accumulated in wheat leaves 96 hours after inoculation with *Bgt*. In *Arabidopsis,* this compound is involved in local and systemic acquired resistance (SAR) against some bacterial pathogens, and is described as an endogenous mediator of defense amplification and priming (Návarová et al., 2012). Increased levels of pipecolic acid and N-Hydroxypipecolic acid were observed in the

primary infected leaves, and both are suggested to travel through vascular tissue to distal secondary leaves, acting such as messengers for SAR establishment (Huang et al., 2020). Pipecolic acid could then orchestrate or regulate SAR via SA-dependent and -independent activation pathways (Bernsdorff et al., 2016). The late accumulation of pipecolic acid observed in infected leaves of the cultivar Pakito, which is moderately susceptible to *Bgt*, suggests its involvement in basal resistance against this fungal pathogen, and its participation in SAR or distal increased resistance has to be studied.

The metabolomic analyses highlight the central role of the phenylpropanoid pathway in defense in wheat challenged by powdery mildew. In the phenylpropanoid biosynthesis pathway, PAL is the upstream enzyme which converts phenylalanine to trans-cinnamic acid. This compound which can serve as a precursor of SA, can be allocated for flavonoids, or various hydroxycinnamic acids biosynthesis, in different shunts of the phenylpropanoid pathway. In our study, no accumulation of flavonoids was observed, which is consistent with the lack of CHS up-regulation. However, PAL was over-expressed, and phenylalanine and HCAAs accumulated between the second and the fourth days following inoculation. HCAAs (also known as phenylamides or phenolamides) are amides of hydroxycinnamic or benzoic acids, linked with various amines, such as agmatine or putrescine. In our study, HCAAs accumulation was first highlighted by a targeted metabolomic approach applied to compounds previously identified in wheat leaves. Furthermore, the non-targeted metabolomic analysis applied to the same samples showed that many of the major ions accumulated in response to Bgt inoculation were actually derived from HCAAs while other defense-related metabolites such as benzoxazinoids remain relatively unaffected.

Altogether, our results indicate that HCAAs accumulation is a major metabolic response of the Pakito wheat cultivar subjected to *Bgt* inoculation. During biotic stresses, these secondary metabolites accumulate mainly but not exclusively in resistant plants following microbial infection, then suggesting their role in quantitative -or non-specific- resistance (Morimoto et al., 2018; von Röpenack et al., 1998). In our experiments, caffeoyl agmatine, coumaroyl agmatine, feruoyl agmatine and sinapoyl agmatine accumulated in susceptible wheat leaves from 48h after inoculation with *Bgt*, as well as caffeoyl putrescine and feruloyl putrescine. Similarly, HCAAs containing agmatine and putrescine as amine component, such as coumaroyl agmatine, feruoyl agmatine, feruoyl putrescine and coumaroyl putrescine, were induced in wheat in response to *Bipolaris sorokiniana*, the causal agent of spot blotch of *Poaceae* species (Ube et al., 2019). In addition, other HCAAs than those identified in our study accumulated, like p-coumaric acid amides of hydroxyputrescine, hydroxyagmatine, hydroxydehydroagmatine, N-cinnamoyl-9-hydroxy-8-oxotryptamine and N-cinnamoyl-8-oxotryptamine, the two last ones being considered as phytoalexins (Ube et al., 2019). Such compounds and HCAAs in general could be to investigate in our pathosytem in response to resistance induction by various biosourced molecules or beneficial microorganisms, since they could participate to the observed improvement of quantitative resistance. HCAAs also accumulate during some other compatible plant-fungi interactions, as reported in sugarcane-*Ustilago scitaminea* (Legaz et al., 1998). HCAAs containing agmatine and putrescine as amine component could then be involved in basal-resistance in wheat against *Bgt*. Their protective role could be linked to a direct antimicrobial activity and an involvement in the reinforcement of the cell wall of plants facing the pathogenic agent, *via* a multistep process involving polymerization through a peroxidase activity (Roumani et al., 2020). HCAAs accumulation, in addition

to *POX* and *PR15* overexpression, is consistent with local cell wall reinforcement at the penetration sites of *Bgt*. Moreover, the up-regulation of *WRKY53*, encoding a transcription factor also known as WRKY26 in wheat, confirms the involvement of POX in these first steps of defense. WRKY53 is described to regulate oxidative responses in wheat under stress conditions, targeting a peroxidase (Van Eck et al., 2014). Previous studies noticed that phenolic compounds accumulation in epidermal cell walls is crucial during elicitor-induced resistance in wheat against *Bgt* (Randoux et al., 2010, Renard-Merlier et al., 2007), pointing out the importance of cell wall reinforcement during basal defenses in wheat against *Bgt.* In barley seedlings resistant to *Erysiphe graminis* f. sp. *hordei* (actually *Blumeria graminis* f. sp. *hordei*), the accumulation of p-coumaroyl-hydroxyagmatine was higher in resistant plantlets than in susceptible ones upon fungal penetration attempts; this compound was supposed to participate to papillae formation and effectiveness *via* cross-linking processes. Moreover, exogenous application of p-coumaroyl-hydroxyagmatine also inhibited the formation of haustoria *in vivo*, and the formation of appressoria *in vitro* (Von Röpenack et al., 1998). In some plant species, compounds derived from the isoprenoid pathway, such as monoterpenes, sesquiterpenes, diterpenes and sterols are involved in a broad spectrum of defense mechanisms from direct effects with their biological activities on pathogens (phytoalexins) to indirect effects acting as signal molecules (specific volatiles compounds) (Singh and Sharma, 2015). On the one hand, 3-Hydroxy-3-methylglutaryl-CoA reductase (HMGR), the key enzyme that catalyzes essential regulatory steps of the mevalonic acid pathway, is considered as the first rate-limiting enzyme in cytosolic isoprenoid biosynthesis (Gu et al., 2015; Block et al., 2019). On the other hand, Farnesyl pyrophosphate synthase (FPPS) and (E, E)-alpha-farnesene synthase (FAR), both related to sesquiterpene biosynthesis, produce volatile

525 compounds to repel pest or attract pest predators (Zhang et al., 2015; Lin et al., 2017).
526 In the susceptible wheat cultivar Pakito, *Bgt* inoculation resulted in a down regulation
527 of *FAR* and a transient upregulation of *HMGR*. This limited upregulation of *HMGR* is
528 consistent with the fact that wheat has not been found to accumulate significant
529 amounts of terpenoid phytoalexins, unlike other *Poaceae* such as rice (*Oryza sativa*)
530 or maize (*Zea mays*) (Ube et al., 2019).
531
532 In our study, RT-qPCR and metabolomics were used to assay, respectively, some
533 defense genes expression and metabolites accumulation in a cultivar of wheat
534 moderately susceptible to *Bgt* during the first days after inoculation. Pakito wheat
535 exhibited a specific pattern of expression of PR-proteins sharing mainly direct
536 antimicrobial activities, including *PR1*, *PR4*, *PR5* and *PR8,* which were continuously
537 up-regulated and strengthened over the two first days of infection, while other defense-
538 related genes were more transiently over-expressed at the beginning of the infection
539 with *Bgt*. Among these genes, some genes in the phenylpropanoid pathway exhibited
540 a significant up-regulation, which was later followed by HCAAs accumulation. HCAAs
541 accumulated concomitantly with an oxalate oxidase (*PR15*) and a peroxidase (*POX*)
542 gene induction in wheat leaves, which could participate to cell wall reinforcement at
543 the penetration sites of the fungus. Pipecolic acid accumulation suggested a SA-
544 mediated signalization. Both transcriptomic and metabolomic analyses pointed out the
545 biosynthesis of HCAAs as a major response to *Bgt* infection in the Pakito cultivar.
546 These new insights lead to a better understanding of basal defense mechanisms taking
547 place in wheat leaves throughout the first days after *Bgt* inoculation. Pakito wheat
548 cultivar being moderately susceptible, some of these defense mechanisms related to
549 PAMP-triggered immunity (PTI) maybe not sufficient or inactivated consequently to the

550 release of some effectors by the pathogen fungus, leading to ETS (Effector-Triggered
551 Susceptibility). Nevertheless, the induction of similar mechanisms in PTI and ETI
552 becomes more and more evident (Yuan et al., 2021). Such results will be very useful
553 to develop new tools and biomarkers for evaluating biocontrol treatments aiming to
554 induce plant defense and to enhance resistance.
555
556
557 **REFERENCES**

558 Benjamini, Y., and Hochberg, Y. 1995. Controlling the False Discovery Rate: A
559 practical and powerful approach to multiple testing. Journal of the Royal Statistical
560 Society: Series B (Methodological). 57:289–300.

561 Bernsdorff, F., Döring, A.-C., Gruner, K., Schuck, S., Bräutigam, A., and Zeier, J. 2016.
562 Pipecolic acid orchestrates plant systemic acquired resistance and defense priming via
563 salicylic acid-dependent and -independent pathways. Plant Cell. 28:102–129.

564 Block, A. K., Vaughan, M. M., Schmelz, E. A., and Christensen, S. A. 2019.
565 Biosynthesis and function of terpenoid defense compounds in maize (Zea mays).
566 Planta. 249:21–30.

567 Brisset, M.-N., and Dugé de Bernonville, T. 2011. Device for determining or studying
568 the state of stimulation of the natural defences of plants or portions of plants.

569 Chen, X. M., Luo, Y. H., Xia, X. C., Xia, L. Q., Chen, X., Ren, Z. L., et al. 2005.
570 Chromosomal location of powdery mildew resistance gene Pm16 in wheat using SSR
571 marker analysis. Plant Breeding. 124:225–228.

572 Dangl, J. L., and Jones, J. D. 2001. Plant pathogens and integrated defence responses
573 to infection. Nature. 411:826–833.

De Borba, M. C., Velho, A. C., Maia-Grondard, A., Baltenweck, R., Magnin-Robert, M., Randoux, B., et al. 2021. The algal polysaccharide ulvan induces resistance in wheat against Zymoseptoria tritici without major alteration of leaf metabolome. Front. Plant Sci. 12:703712.

De Bruijn, W. J. C., Vincken, J.-P., Duran, K., and Gruppen, H. 2016. Mass spectrometric characterization of benzoxazinoid glycosides from Rhizopus-elicited wheat (Triticum aestivum) seedlings. J Agric Food Chem. 64:6267–6276De Bruijn, W. J. C., Gruppen, H., Vincken, J. P. 2018. Structure and biosynthesis of benzoxazinoids: Plant defence metabolites with potential as antimicrobial scaffolds. *Phytochemistry* 155:233-243. doi: 10.1016/j.phytochem.2018.07.005.

Dugé de Bernonville, T., Marolleau, B., Staub, J., Gaucher, M., and Brisset, M.-N. 2014. Using molecular tools to decipher the complex world of plant resistance inducers: an apple case study. J Agric Food Chem. 62:11403–11411.

Enoki, S., and Suzuki, S. 2016. Pathogenesis-related proteins in grape. In *Grape and Wine Biotechnology*, eds. Antonio Morata and Iris Loira. Rijeka: IntechOpen. Available at: https://doi.org/10.5772/64873.

FAO. 2018. *Global Information and Early Warning System on Food and Agriculture (GIEWS). Rome: Food and Agriculture Organization of the United Nations (FAO)*. Food and Agriculture Organization of the United Nations (FAO).

Gao, H., Niu, J., and Li, S. 2018. Impacts of wheat powdery mildew on grain yield & quality and its prevention and control methods. American Journal of Agriculture and Forestry. 6:141–147.

Geddes, J., Eudes, F., Laroche, A., and Selinger, L. B. 2008. Differential expression of proteins in response to the interaction between the pathogen Fusarium graminearum and its host, Hordeum vulgare. Proteomics. 8:545–554.

Gu, W., Geng, C., Xue, W., Wu, Q., Chao, J., Xu, F., et al. 2015. Characterization and function of the 3-hydroxy-3-methylglutaryl-CoA reductase gene in Alisma orientale (Sam.) Juz. and its relationship with protostane triterpene production. Plant Physiology and Biochemistry. 97:378–389.

Gunnaiah, R., Kushalappa, A. C., Duggavathi, R., Fox, S., Somers, D. J. 2012. Integrated metabolo-proteomic approach to decipher the mechanisms by which wheat QTL (Fhb1) contributes to resistance against Fusarium graminearum. *PLoS One*. 7(7):e40695. doi: 10.1371/journal.pone.0040695.

Hashimoto, Y., Shudo, K. 1996. Chemistry of biologically active benzoxazinoids, *Phytochemistry*,43 (3):551-559, ISSN 0031-9422, https://doi.org/10.1016/0031-9422(96)00330-5.

Huang, R.-H., Xiang, Y., Liu, X.-Z., Zhang, Y., Hu, Z., and Wang, D.-C. 2002. Two novel antifungal peptides distinct with a five-disulfide motif from the bark of Eucommia ulmoides Oliv. FEBS Lett. 521:87–90.

Huang, W., Wang, Y., Li, X., and Zhang, Y. 2020. Biosynthesis and regulation of salicylic acid and N-hydroxypipecolic acid in plant immunity. Mol Plant. 13:31–41.

Huang, X.-Q., and Röder, M. S. 2004. Molecular mapping of powdery mildew resistance genes in wheat: A review. Euphytica. 137:203–223.

619 Jin, S., Yoshida, M., Nakajima, T., and Murai, A. 2003. Accumulation of
620 hydroxycinnamic acid amides in winter wheat under snow. Biosci Biotechnol Biochem.
621 67:1245–1249.

622 Jones, J. D. G., and Dangl, J. L. 2006. The plant immune system. Nature. 444:323–
623 329.

624 Katagiri, F. 2004. A global view of defense gene expression regulation--a highly
625 interconnected signaling network. Curr Opin Plant Biol. 7:506–511.

626 Legaz, M. E., Armas, R. de, Piñón, D., and Vicente, C. 1998. Relationships between
627 phenolics-conjugated polyamines and sensitivity of sugarcane to smut (Ustilago
628 scitaminea). Journal of Experimental Botany. 49:1723–1728.

629 Li, H., Dong, Z., Ma, C., Xia, Q., Tian, X., Sehgal, S., et al. 2020. A spontaneous wheat-
630 Aegilops longissima translocation carrying Pm66 confers resistance to powdery
631 mildew. Theor Appl Genet. 133:1149–1159.

632 Li, Z., Zhao, C., Zhao, X., Xia, Y., Sun, X., Xie, W., et al. 2018. Deep annotation of
633 hydroxycinnamic acid amides in plants based on ultra-high-performance liquid
634 chromatography-high-resolution mass spectrometry and its in silico database. Anal
635 Chem. 90:14321–14330.

636 Liljeroth, E., Santén, K., and Bryngelsson, T. 2001. PR protein accumulation in seminal
637 roots of barley and wheat in response to fungal infection - the importance of cortex
638 senescence. Journal of Phytopathology. 149:447–456.

639 Lin, J., Wang, D., Chen, X., Köllner, T. G., Mazarei, M., Guo, H., et al. 2017. An
640 (E,E)-α-farnesene synthase gene of soybean has a role in defence against nematodes

641 and is involved in synthesizing insect-induced volatiles. Plant Biotechnol J. 15:510–
642 519.

643 McIntosh, R. A., Dubcovsky, J., Rogers, W. J., Xia, X. C., and Raupp, W. J. 2019.
644 *Catalogue of gene symbols for wheat: 2019 supplement.* W.J. Raupp. Manhattan (NY).

645 Miedaner, T., Schmidt, H. K., and Geiger, H. H. 1993. Components of variation for
646 quantitative adult-plant resistance to powdery mildew in winter rye. Phytopathology.
647 83:1071–1075.

648 Morimoto, N., Ueno, K., Teraishi, M., Okumoto, Y., Mori, N., and Ishihara, A. 2018.
649 Induced phenylamide accumulation in response to pathogen infection and hormone
650 treatment in rice (Oryza sativa). Biosci Biotechnol Biochem. 82:407–416.

651 Muroi, A., Ishihara, A., Tanaka, C. *et al.* 2009. Accumulation of hydroxycinnamic acid
652 amides induced by pathogen infection and identification of agmatine
653 coumaroyltransferase in *Arabidopsis thaliana*. *Planta* 230:517–527.
654 https://doi.org/10.1007/s00425-009-0960-0

655
656 Mustafa, G., Khong, N. G., Tisserant, B., Randoux, B., Fontaine, J., Magnin-Robert,
657 M., et al. 2017. Defence mechanisms associated with mycorrhiza-induced resistance
658 in wheat against powdery mildew. Functional Plant Biol. 44:443.

659 Mwale, V. M., Chilembwe, E. H. C., and Uluko, H. C. 2014. Wheat powdery mildew
660 (Blumeria graminis f. sp. tritici): Damage effects and genetic resistance developed in
661 wheat (Triticum aestivum). International Research Journal of Plant Science. 5:1–16.

662 Návarová, H., Bernsdorff, F., Döring, A.-C., and Zeier, J. 2012. Pipecolic acid, an
663 endogenous mediator of defense amplification and priming, is a critical regulator of
664 inducible plant immunity. Plant Cell. 24:5123–5141.

665 Nawrot, R., Barylski, J., Nowicki, G., Broniarczyk, J., Buchwald, W., and Goździcka-
666 Józefiak, A. 2014. Plant antimicrobial peptides. Folia Microbiol (Praha). 59:181–196.

667 Niderman, T., Genetet, I., Bruyère, T., Gees, R., Stintzi, A., Legrand, M., Fritig, B.,
668 Mösinger, E. 1995. Pathogenesis-related PR-1 proteins are antifungal. Isolation and
669 characterization of three 14-kilodalton proteins of tomato and of a basic PR-1 of
670 tobacco with inhibitory activity against Phytophthora infestans. Plant Physiol.
671 108(1):17-27.

672
673 Nürnberger, T., Brunner, F., Kemmerling, B., and Piater, L. 2004. Innate immunity in
674 plants and animals: striking similarities and obvious differences. Immunol Rev.
675 198:249–266.

676 Pennington, H. G., Jones, R., Kwon, S., Bonciani, G., Thieron, H., Chandler, T., et al.
677 2019. The fungal ribonuclease-like effector protein CSEP0064/BEC1054 represses
678 plant immunity and interferes with degradation of host ribosomal RNA. PLoS Pathog.
679 15:e1007620.

680 Piarulli, L., Gadaleta, A., Mangini, G., Signorile, M. A., Pasquini, M., Blanco, A., et al.
681 2012. Molecular identification of a new powdery mildew resistance gene on
682 chromosome 2BS from Triticum turgidum ssp. dicoccum. Plant Sci. 196:101–106.

683 Randoux, B., Renard, D., Nowak, E., Sanssené, J., Courtois, J., Durand, R., et al.
684 2006. Inhibition of *Blumeria graminis* f. sp. *tritici* germination and partial enhancement
685 of wheat defenses by Milsana. Phytopathology®. 96:1278–1286.

686 Randoux, B., Renard-Merlier, D., Mulard, G., Rossard, S., Duyme, F., Sanssené, J., et
687 al. 2010. Distinct defenses induced in wheat against powdery mildew by acetylated
688 and nonacetylated oligogalacturonides. Phytopathology. 100:1352–1363.

689 Renard-Merlier, D., Randoux, B., Nowak, E., Farcy, F., Durand, R., and Reignault, P.
690 2007. Iodus 40, salicylic acid, heptanoyl salicylic acid and trehalose exhibit different
691 efficacies and defence targets during a wheat/powdery mildew interaction.
692 Phytochemistry. 68:1156–1164.

693 Roumani, M., Besseau, S., Gagneul, D., Robin, C., and Larbat, R. 2021. Phenolamides
694 in plants: an update on their function, regulation, and origin of their biosynthetic
695 enzymes. J Exp Bot. 72:2334–2355.

696 Schmittgen, T. D., and Livak, K. J. 2008. Analyzing real-time PCR data by the
697 comparative CT method. Nat Protoc. 3:1101–1108.

698 Shoresh, M., and Harman, G. E. 2008. Genome-wide identification, expression and
699 chromosomal location of the genes encoding chitinolytic enzymes in Zea mays. Mol
700 Genet Genomics. 280:173–185.

701 Singh, B., and Sharma, R. A. 2015. Plant terpenes: defense responses, phylogenetic
702 analysis, regulation and clinical applications. 3 Biotech. 5:129–151.

703 Singh, R., Tiwari, J. K., Sharma, V., Singh, B. P., and Rawat, S. 2014. Role of Pathogen
704 related protein families in defence mechanism with potential role in applied
705 biotechnology. International Journal of Advanced Research. 2:210–226.

706 Smith, C. A., Want, E. J., O'Maille, G., Abagyan, R., and Siuzdak, G. 2006. XCMS:
707 processing mass spectrometry data for metabolite profiling using nonlinear peak
708 alignment, matching, and identification. Anal Chem. 78:779–787.

709 Tayeh, Ch., Randoux, B., Tisserant, B., Khong, G., Jacques, Ph., and Reignault, Ph.
710 2015. Are ineffective defence reactions potential target for induced resistance during

711 the compatible wheat-powdery mildew interaction? Plant Physiology and Biochemistry.
712 96:9–19.

713 Thaler, J. S., Humphrey, P. T., Whiteman, N. K. 2012. Evolution of jasmonate and
714 salicylate signal crosstalk. Trends Plant Sci. 17:260–270. doi:
715 10.1016/j.tplants.2012.02.010

716
717 Ube, N., Harada, D., Katsuyama, Y., Osaki-Oka, K., Tonooka, T., Ueno, K., et al. 2019.
718 Identification of phenylamide phytoalexins and characterization of inducible
719 phenylamide metabolism in wheat. Phytochemistry. 167:112098.

720 Van Eck, L., Davidson, R. M., Wu, S., Zhao, B. Y., Botha, A.-M., Leach, J. E., et al.
721 2014. The transcriptional network of WRKY53 in cereals links oxidative responses to
722 biotic and abiotic stress inputs. Funct Integr Genomics. 14:351–362.

723 Voll, L. M., Horst, R. J., Voitsik, A.-M., Zajic, D., Samans, B., Pons-Kühnemann, J., et
724 al. 2011. Common motifs in the response of cereal primary metabolism to fungal
725 pathogens are not based on similar transcriptional reprogramming. Front Plant Sci.
726 2:39.

727 Von Röpenack, E., Parr, A., and Schulze-Lefert, P. 1998. Structural analyses and
728 dynamics of soluble and cell wall-bound phenolics in a broad-spectrum resistance to
729 the powdery mildew fungus in barley. J Biol Chem. 273:9013–9022.

730 Walters, D. R., Ratsep, J., and Havis, N. D. 2013. Controlling crop diseases using
731 induced resistance: challenges for the future. Journal of Experimental Botany.
732 64:1263–1280.

733 Wang, J. M., Liu, H.Y., Xu, H. M. *et al.* 2012. Analysis of differential transcriptional
734 profiling in wheat infected by *Blumeria graminis* f. sp. *tritici* using GeneChip. Mol Biol
735 Rep 39:381–387. https://doi.org/10.1007/s11033-011-0749-7

736 Wojakowska, A., Perkowski, J., Góral, T., and Stobiecki, M. 2013. Structural
737 characterization of flavonoid glycosides from leaves of wheat (Triticum aestivum L.)
738 using LC/MS/MS profiling of the target compounds. J Mass Spectrom. 48:329–339.

739 Wu, S., Wang, H., Yang, Z., and Kong, L. 2014. Expression comparisons of
740 Pathogenesis-Related (PR) genes in wheat in response to infection/infestation by
741 Fusarium, Yellow dwarf virus (YDV) Aphid-Transmitted and Hessian Fly. Journal of
742 Integrative Agriculture. 13:926–936.

743 Yogendra, K. N., Pushpa, D., Mosa, K. A., Kushalappa, A. C., Murphy, A., and
744 Mosquera, T. 2014. Quantitative resistance in potato leaves to late blight associated
745 with induced hydroxycinnamic acid amides. Funct. Integr. Genomics. 14:285–298. doi:
746 10.1007/s10142-013-0358-8

747
748 Yuan, M., Ngou, B. P. M., Ding, P., and Xin, X.-F. 2021. PTI-ETI crosstalk: an
749 integrative view of plant immunity. Curr Opin Plant Biol. 62:102030.

750 Zhang, Y., Li, Z.-X., Yu, X.-D., Fan, J., Pickett, J. A., Jones, H. D., et al. 2015. Molecular
751 characterization of two isoforms of a farnesyl pyrophosphate synthase gene in wheat
752 and their roles in sesquiterpene synthesis and inducible defence against aphid
753 infestation. New Phytol. 206:1101–1115.

754 Zhu, T., Wu, L., He, H., Song, J., Jia, M., Liu, L., et al. 2020. Bulked segregant RNA-
755 Seq reveals distinct expression profiling in chinese wheat cultivar Jimai 23 responding
756 to powdery mildew. Front Genet. 11:474.

Zipfel, C., and Felix, G. 2005. Plants and animals: a different taste for microbes? Curr Opin Plant Biol. 8:353–360.

Figure captions

Figure 1. Profile of defense gene expression, monitored at 24h and 48h following the inoculation of wheat with *B. graminis* f.sp. *tritici* (*Bgt*). Average defense gene expression was obtained by the $2^{\wedge(-\Delta\Delta Ct)}$ calculation method expressed in log2 fold change, using *Bgt*-infected plants compared to non-infected control plants for each time point, using 3 biological replicates corresponding to first leaves from 3 different plants. Defense gene expression fold changes are given by shades of red or blue colors according to the scale bar and two experiments (Exp.1 and Exp.2) were performed to confirm the results.

Figure 2. Global wheat leaf metabolite changes following inoculation with *B. graminis* f.sp. *tritici*. Principal component analysis was performed on all compounds quantified in the targeted analysis, in all conditions and time points. Data represent nine biological replicates for each condition and time point. The shown principal components explain respectively 21.3% and 21.1% of the variance separating the six groups of plants.

Figure 3. Heatmap of significant wheat leaf metabolite changes following inoculation with *B. graminis* f.sp. *tritici*. Wheat plants were mock infected (NI) or infected (I) with *Bgt*. Log2 of significant metabolite fold changes for I/NI pairwise comparisons at 24,

48, 72 and 96 hpi are given by shades of red or blue colors according to the scale bar. Metabolites were grouped according to their chemical family as amino acids (AA), benzoxazinoids (BZ), flavonoids (F), hormones (H), hydroxycinnamic acid amides (HCAA) and amines (N). Data represent mean values of nine biological replicates for each condition and time point. Statistical analysis was performed using Tukey's Honest Significant Difference method followed by a false discovery rate (FDR) correction, with FDR < 0.05. For FDR ≥ 0.05, log2 fold changes were set to 0.

Figure 4. Effects of *Blumeria graminis* f.sp. *tritici* inoculation on histidine (**a**), glutamine (**b**), phenylalanine (**c**) and pipecolic acid (**d**) accumulation in wheat leaves. Infected (I) and non-infected (NI) leaves were collected at 24, 48, 72 and 96 hpi. The histograms represent mean values (± standard errors) obtained for nine samples per condition, from three experiments (three samples per experiment). Columns headed by different letters indicate statistically significant differences between the different conditions (ANOVA, test post-hoc multiple Bonferroni, P ≤ 0.05).

Figure 5. Non-targeted analysis of wheat leaf metabolite changes following inoculation with *B. graminis* f.sp. *tritici* (*Bgt*).

Ions of interest were selected based on a significant differential accumulation between *Bgt*-infected and control wheat leaves at 48 hpi, with a fold change > 2. Log2 of significant ion fold changes for I/NI pairwise comparisons at 24, 48, 72 and 96 hpi are given by shades of red or blue colors according to the scale bar. Statistical analysis was performed using Tukey's HSD method followed by a FDR correction, with FDR <

0.05. For FDR ≥ 0.05, log2 fold changes were set to 0. Putative identification of the metabolites corresponding to the indicated ions are the following: 1: Hydroxytyrosine, 2: Coumaroyl-hydroxyputrescine, 3: Feruloyl-hydroxyputrescine, 4: Coumaroyl-hydroxyagmatine, 5: Coumaroyl-hydroxy-dehydroagmatine, 6: Feruloylputrescine, 7: Feruloyl-hydroxyagmatine, 8: Feruloyl-hydroxydehydroagmatine, 9: Coumaroylagmatine, 10: Feruloylagmatine, 11: Coumaroyl-dehydroagmatine, 12: Sinapoylagmatine, 13: Dodecanamine. Characteristics of all ions are presented in Supplemental Table 3.

Figure 6. Biosynthetic pathway of the main HCAAs accumulating following inoculation of wheat cv. Pakito with *Bgt*, based on non-targeted analysis of major differentially accumulated ions. Metabolites indicated in red were putatively identified based expertized analysis of high-resolution mass spectra and comparison with published literature. For each metabolite, log2 of significant ion fold changes for I/NI pairwise comparisons at 24, 48, 72 and 96 hpi are given by shades of red or blue colors according to the scale bar (data from Fig. 5).

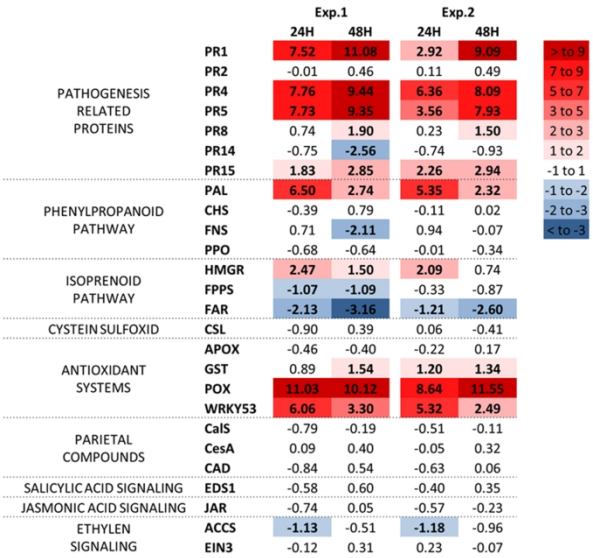

		Exp.1		Exp.2	
		24H	48H	24H	48H
PATHOGENESIS RELATED PROTEINS	PR1	7.52	11.08	2.92	9.09
	PR2	-0.01	0.46	0.11	0.49
	PR4	7.76	9.44	6.36	8.09
	PR5	7.73	9.35	3.56	7.93
	PR8	0.74	1.90	0.23	1.50
	PR14	-0.75	-2.56	-0.74	-0.93
	PR15	1.83	2.85	2.26	2.94
PHENYLPROPANOID PATHWAY	PAL	6.50	2.74	5.35	2.32
	CHS	-0.39	0.79	-0.11	0.02
	FNS	0.71	-2.11	0.94	-0.07
	PPO	-0.68	-0.64	-0.01	-0.34
ISOPRENOID PATHWAY	HMGR	2.47	1.50	2.09	0.74
	FPPS	-1.07	-1.09	-0.33	-0.87
	FAR	-2.13	-3.16	-1.21	-2.60
CYSTEIN SULFOXID	CSL	-0.90	0.39	0.06	-0.41
ANTIOXIDANT SYSTEMS	APOX	-0.46	-0.40	-0.22	0.17
	GST	0.89	1.54	1.20	1.34
	POX	11.03	10.12	8.64	11.55
	WRKY53	6.06	3.30	5.32	2.49
PARIETAL COMPOUNDS	CalS	-0.79	-0.19	-0.51	-0.11
	CesA	0.09	0.40	-0.05	0.32
	CAD	-0.84	0.54	-0.63	0.06
SALICYLIC ACID SIGNALING	EDS1	-0.58	0.60	-0.40	0.35
JASMONIC ACID SIGNALING	JAR	-0.74	0.05	-0.57	-0.23
ETHYLEN SIGNALING	ACCS	-1.13	-0.51	-1.18	-0.96
	EIN3	-0.12	0.31	0.23	-0.07

Figure 1. Profile of defense gene expression, monitored at 24h and 48h following the inoculation of wheat with B. graminis f.sp. tritici (Bgt). Average defense gene expression was obtained by the 2^(-ΔΔCt) calculation method expressed in log2 fold change, using Bgt-infected plants compared to non-infected control plants for each time point, using 3 biological replicates corresponding to first leaves from 3 different plants. Defense gene expression fold changes are given by shades of red or blue colors according to the scale bar and two experiments (Exp.1 and Exp.2) were performed to confirm the results.

861x484mm (118 x 118 DPI)

Figure 2. Global wheat leaf metabolite changes following inoculation with B. graminis f.sp. tritici. Principal component analysis was performed on all compounds quantified in the targeted analysis, in all conditions and time points. Data represent nine biological replicates for each condition and time point. The shown principal components explain respectively 21.3% and 21.1% of the variance separating the six groups of plants.

1749x2475mm (72 x 72 DPI)

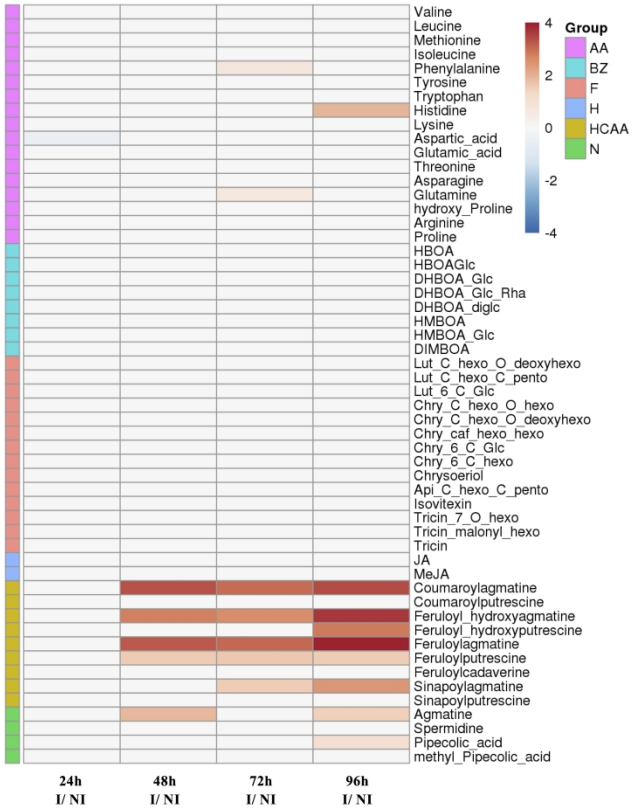

Figure 3. Heatmap of significant wheat leaf metabolite changes following inoculation with B. graminis f.sp. tritici. Wheat plants were mock infected (NI) or infected (I) with Bgt. Log2 of significant metabolite fold changes for I/NI pairwise comparisons at 24, 48, 72 and 96 hpi are given by shades of red or blue colors according to the scale bar. Metabolites were grouped according to their chemical family as amino acids (AA), benzoxazinoids (BZ), flavonoids (F), hormones (H), hydroxycinnamic acid amides (HCAA) and amines (N). Data represent mean values of nine biological replicates for each condition and time point. Statistical analysis was performed using Tukey's Honest Significant Difference method followed by a false discovery rate (FDR) correction, with FDR < 0.05. For FDR ≥ 0.05, log2 fold changes were set to 0.

1749x2475mm (72 x 72 DPI)

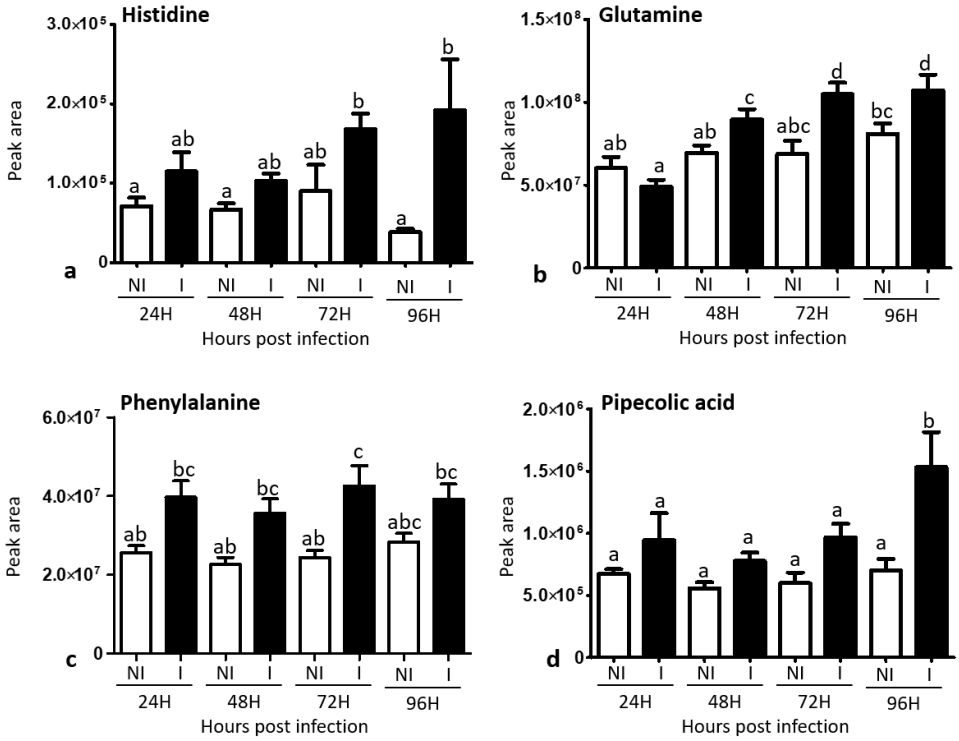

Figure 4. Effects of Blumeria graminis f.sp. tritici inoculation on histidine (a), glutamine (b), phenylalanine (c) and pipecolic acid (d) accumulation in wheat leaves. Infected (I) and non-infected (NI) leaves were collected at 24, 48, 72 and 96 hpi. The histograms represent mean values (± standard errors) obtained for nine samples per condition, from three experiments (three samples per experiment). Columns headed by different letters indicate statistically significant differences between the different conditions (ANOVA, test post-hoc multiple Bonferroni, $P \leq 0.05$).

524x400mm (59 x 59 DPI)

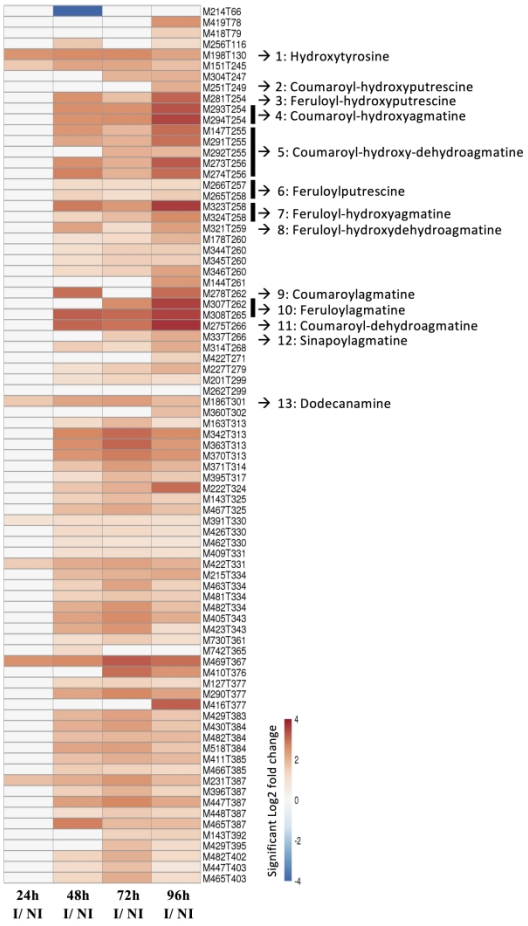

Figure 5. Non-targeted analysis of wheat leaf metabolite changes following inoculation with B. graminis f.sp. tritici (Bgt). Ions of interest were selected based on a significant differential accumulation between Bgt-infected and control wheat leaves at 48 hpi, with a fold change > 2. Log2 of significant ion fold changes for I/NI pairwise comparisons at 24, 48, 72 and 96 hpi are given by shades of red or blue colors according to the scale bar. Statistical analysis was performed using Tukey's HSD method followed by a FDR correction, with FDR < 0.05. For FDR ≥ 0.05, log2 fold changes were set to 0. Putative identification of the metabolites corresponding to the indicated ions are the following: 1: Hydroxytyrosine, 2: Coumaroyl-hydroxyputrescine, 3: Feruloyl-hydroxyputrescine, 4: Coumaroyl-hydroxyagmatine, 5: Coumaroyl-hydroxy-dehydroagmatine, 6: Feruloylputrescine, 7: Feruloyl-hydroxyagmatine, 8: Feruloyl-hydroxydehydroagmatine, 9: Coumaroylagmatine, 10: Feruloylagmatine, 11: Coumaroyl-dehydroagmatine, 12: Sinapoylagmatine, 13: Dodecanamine. Characteristics of all ions are presented in Supplemental Table 3.

1749x2475mm (72 x 72 DPI)

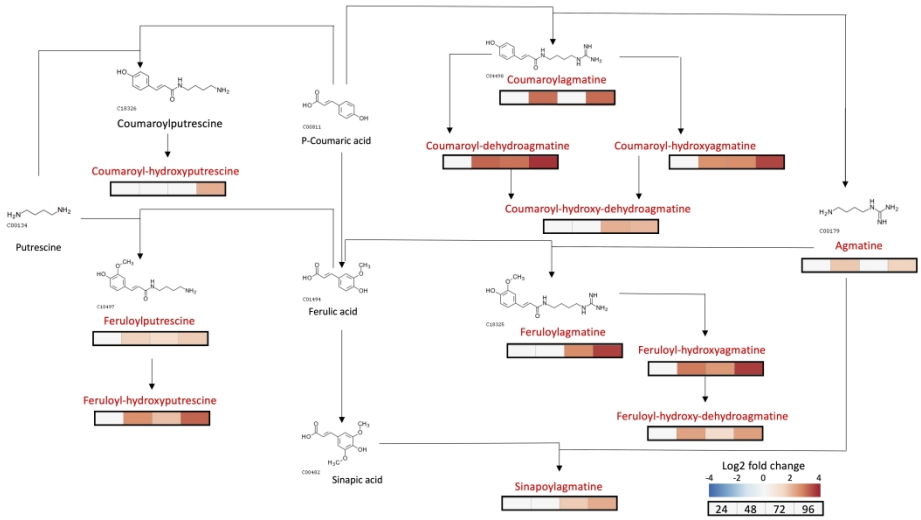

Figure 6. Biosynthetic pathway of the main HCAAs accumulating following inoculation of wheat cv. Pakito with Bgt, based on non-targeted analysis of major differentially accumulated ions. Metabolites indicated in red were putatively identified based expertized analysis of high-resolution mass spectra and comparison with published literature. For each metabolite, log2 of significant ion fold changes for I/NI pairwise comparisons at 24, 48, 72 and 96 hpi are given by shades of red or blue colors according to the scale bar (data from Fig. 5).

2475x1749mm (72 x 72 DPI)

Supplemental Table 1. Twenty-six wheat defense-related genes selected for real time qPCR analyses.

DEFENSE MECHANISMS	GENE	ENZYME	FUNCTION
PATHOGENESIS RELATED PROTEINS	PR1	Pathogenesis-related protein 1	Involved in antimicrobial functions and plant defense signal intensification (Breen et al. 2016)
	PR2	Pathogenesis-related protein 2 (beta 1,3-glucanase)	Cleaves the α-1,3-glucan, one of the major cell wall polysaccharides in filamentous fungi (Sudisha et al. 2012; Yoshimi et al. 2017)
	PR4	Pathogenesis-related protein 4 (hevein-like)	Production of plant antimicrobial peptides (AMPs) acting on cell walls of pathogens (Sudisha et al. 2012)
	PR5	Pathogenesis-related protein 5 (thaumatin-like, osmotin)	Causes leakage of cell constituents from the fungal hyphae and increases the uptake of anti-fungal proteins (Sudisha et al. 2012)
	PR8	Pathogenesis-related protein 8 (class I chitinase)	Acts as a disruptor of fungi cell wall (Sudisha et al. 2012)
	PR14	Pathogenesis-related protein 14 (lipid transfer protein)	Associated to the cell wall, promotes lipid loading and transfer (Sudisha et al. 2012)
	PR15	Pathogenesis-related protein 15 (oxalate oxidase)	Contributes to reactive oxygen species production directly after pathogen infection (Sudisha et al. 2012)
PHENYLPROPANOID PATHWAY	PAL	Phenylalanine ammonia-lyase	Acts as a positive regulator of salicylic acid signalling to cope with microbial pathogens through its enzymatic activity in the phenylpropanoid pathway (Kim and Hwang 2014)
	CHS	Chalcone synthase	Involved in the salicylic acid defense pathway through its role in the flavonoid/isoflavonoid biosynthesis pathway (Dao et al. 2011)
	FNS	Flavone synthase	Serves as potential antioxidants with antimicrobial and insecticidal activities (phytoalexins) (Du et al. 2010)
	PPO	Polyphenol oxidase	Contributes to insect herbivore and pathogen resistance (Constabel and Barbehenn 2008)
ISOPRENOID PATHWAY	HMGR	Hydroxymethyl glutarate-CoA reductase	Involved in the mevalonate pathway that allows biosynthesis of terpenoid defense compounds (Block et al. 2019; Gu et al. 2015)
	FPPS	Farnesyl pyrophosphate synthase	Involved in sesquiterpenes biosynthesis that repel pests (Block et al. 2019; Zhang et al. 2015)
	FAR	(E,E)-alpha-farnesene synthase	Role in defence against nematodes and insects (Lin et al. 2017)
CYSTEIN SULFOXID	CSL	Alliinase	Participates to inhibit the proliferation of both bacteria and fungi (Borlinghaus et al. 2014)
ANTIOXIDANT SYSTEMS	APOX	Ascorbate peroxidase	Protects plant cells against ROS accumulation during adverse environmental conditions (Caverzan et al. 2012)
	GST	Glutathion S-transferase	Role in plant responses during biotic stresses through regulating stress-related gene expression and early signaling events linked to plant defense (Dubreuil-Maurizi and Poinssot 2012)
	POX	Peroxidase	Participates to lignin and suberin formation, synthesis of phytoalexins, metabolism of ROS (reactive oxygen species) and RNS (reactive nitrogen species) acting on the hypersensitive response. (Almagro et al. 2009)
	WRKY	WRKY transcription factor 53	Involved in the regulation of oxidative responses to a wide array of stresses, such as biotic stress in wheat (Van Eck et al. 2014)
PARIETAL COMPOUNDS	CalS	Callose synthase	Takes part to papilla formation during microbial pathogen intrusion (Voigt 2014)
	CesA	Cellulose synthase A	Synthesizes cellulose at the primary cell wall adapting plant growth to environmental stresses and producing DAMPs (Kesten et al. 2017)
	CAD	Cinnamyl alcohol dehydrogenase	Contributes to plant resistance through its regulation of the expression of defense genes and monolignol biosynthesis-related genes (Rong et al. 2016)
SALICYLIC ACID SIGNALING	EDS1	Disease resistance protein EDS1	Mediates resistance response through salicylic acid signaling (Falk et al. 1999; Rustérucci et al. 2001)
JASMONIC ACID SIGNALING	JAR	Jasmonate resistant 1	Involved in jasmonate synthesis to allow jasmonic acid signaling in response to biotic/abiotic stresses (Kazan and Manners 2008; Riemann et al. 2008)
ETHYLEN SIGNALING	ACCS	1-aminocyclopropane-1-carboxylate synthase	Role in plant immunity through ethylene signaling (Yang et al. 2019)
	EIN3	EIN3-Binding F Box Protein 1	Mitigates the oxidative stress (Asensi-Fabado et al. 2012)

Almagro, L., Gómez Ros, L. V., Belchi-Navarro, S., Bru, R., Ros Barceló, A., and Pedreño, M. A. 2009. Class III peroxidases in plant defence reactions. J Exp Bot. 60:377–390.

Asensi-Fabado, M. A., Cela, J., Müller, M., Arrom, L., Chang, C., and Munné-Bosch, S. 2012. Enhanced oxidative stress in the ethylene-insensitive (ein3-1) mutant of Arabidopsis thaliana exposed to salt stress. J Plant Physiol. 169:360–368.

Block, A. K., Vaughan, M. M., Schmelz, E. A., and Christensen, S. A. 2019. Biosynthesis and function of terpenoid defense compounds in maize (Zea mays). Planta. 249:21–30.

Borlinghaus, J., Albrecht, F., Gruhlke, M. C. H., Nwachukwu, I. D., and Slusarenko, A. J. 2014. Allicin: chemistry and biological properties. Molecules. 19:12591–12618.

Breen, S., Williams, S. J., Winterberg, B., Kobe, B., and Solomon, P. S. 2016. Wheat PR-1 proteins are targeted by necrotrophic pathogen effector proteins. The Plant Journal. 88:13–25.

Caverzan, A., Passaia, G., Rosa, S. B., Ribeiro, C. W., Lazzarotto, F., and Margis-Pinheiro, M. 2012. Plant responses to stresses: Role of ascorbate peroxidase in the antioxidant protection. Genet Mol Biol. 35:1011–1019.

Constabel, C. P., and Barbehenn, R. 2008. Defensive Roles of Polyphenol Oxidase in Plants. In *Induced Plant Resistance to Herbivory*, ed. Andreas Schaller. Dordrecht: Springer Netherlands, p. 253–270. Available at: http://link.springer.com/10.1007/978-1-4020-8182-8_12 [Accessed August 26, 2022].

Dao, T. T. H., Linthorst, H. J. M., and Verpoorte, R. 2011. Chalcone synthase and its functions in plant resistance. Phytochem Rev. 10:397–412.

Du, Y., Chu, H., Wang, M., Chu, I. K., and Lo, C. 2010. Identification of flavone phytoalexins and a pathogen-inducible flavone synthase II gene (SbFNSII) in sorghum. Journal of Experimental Botany. 61:983–994.

Dubreuil-Maurizi, C., and Poinssot, B. 2012. Role of glutathione in plant signaling under biotic stress. Plant Signal Behav. 7:210–212.

Falk, A., Feys, B. J., Frost, L. N., Jones, J. D., Daniels, M. J., and Parker, J. E. 1999. EDS1, an essential component of R gene-mediated disease resistance in Arabidopsis has homology to eukaryotic lipases. Proc Natl Acad Sci U S A. 96:3292–3297.

Gu, W., Geng, C., Xue, W., Wu, Q., Chao, J., Xu, F., et al. 2015. Characterization and function of the 3-hydroxy-3-methylglutaryl-CoA reductase gene in Alisma orientale (Sam.) Juz. and its relationship with protostane triterpene production. Plant Physiology and Biochemistry. 97:378–389.

Kazan, K., and Manners, J. M. 2008. Jasmonate Signaling: Toward an Integrated View. Plant Physiol. 146:1459–1468.

Kesten, C., Menna, A., and Sánchez-Rodríguez, C. 2017. Regulation of cellulose synthesis in response to stress. Curr Opin Plant Biol. 40:106–113.

Kim, D. S., and Hwang, B. K. 2014. An important role of the pepper phenylalanine ammonia-lyase gene (PAL1) in salicylic acid-dependent signalling of the defence response to microbial pathogens. J Exp Bot. 65:2295–2306.

Lin, J., Wang, D., Chen, X., Köllner, T. G., Mazarei, M., Guo, H., et al. 2017. An (E,E)-α-farnesene synthase gene of soybean has a role in defence against nematodes and is involved in synthesizing insect-induced volatiles. Plant Biotechnol J. 15:510–519.

Riemann, M., Riemann, M., and Takano, M. 2008. Rice JASMONATE RESISTANT 1 is involved in phytochrome and jasmonate signalling. Plant Cell Environ. 31:783–792.

Rong, W., Luo, M., Shan, T., Wei, X., Du, L., Xu, H., et al. 2016. A Wheat Cinnamyl Alcohol Dehydrogenase TaCAD12 Contributes to Host Resistance to the Sharp Eyespot Disease. Frontiers in Plant Science. 7 Available at: https://www.frontiersin.org/articles/10.3389/fpls.2016.01723 [Accessed August 26, 2022].

Rustérucci, C., Aviv, D. H., Holt, B. F., Dangl, J. L., and Parker, J. E. 2001. The disease resistance signaling components EDS1 and PAD4 are essential regulators of the cell death pathway controlled by LSD1 in Arabidopsis. Plant Cell. 13:2211–2224.

Sudisha, J., Sharathchandra, R. G., Amruthesh, K. N., Kumar, A., and Shetty, H. S. 2012. Pathogenesis Related Proteins in Plant Defense Response. In *Plant Defence: Biological Control*, , p. 379–403. Available at: https://app.dimensions.ai/details/publication/pub.1036536464.

Van Eck, L., Davidson, R. M., Wu, S., Zhao, B. Y., Botha, A.-M., Leach, J. E., et al. 2014. The transcriptional network of WRKY53 in cereals links oxidative responses to biotic and abiotic stress inputs. Funct Integr Genomics. 14:351–362.

Voigt, C. A. 2014. Callose-mediated resistance to pathogenic intruders in plant defense-related papillae. Front Plant Sci. 5:168.

Yang, B., Wang, Y., Guo, B., Jing, M., Zhou, H., Li, Y., et al. 2019. The Phytophthora sojae RXLR effector Avh238 destabilizes soybean Type2 GmACSs to suppress ethylene biosynthesis and promote infection. New Phytologist. 222:425–437.

Yoshimi, A., Miyazawa, K., and Abe, K. 2017. Function and Biosynthesis of Cell Wall α-1,3-Glucan in Fungi. Journal of Fungi. 3:63.

Zhang, Y., Li, Z.-X., Yu, X.-D., Fan, J., Pickett, J. A., Jones, H. D., et al. 2015. Molecular characterization of two isoforms of a farnesyl pyrophosphate synthase gene in wheat and their roles in sesquiterpene synthesis and inducible defence against aphid infestation. New Phytol. 206:1101–1115.

Supplemental Table 2. List of the 53 metabolites from wheat leaves selected for targeted metabolomic analyses. Metabolites were classified according to KEGG (Kyoto Encyclopedia of Genes and Genomes; http://www.genome.ad.jp/kegg) and PubChem (http://pubchem.ncbi.nlm.nih.gov) databases. Id: identifier; *m/z*: mass-to-charge ratio; *m/z* error (difference between the measured *m/z* and the calculated *m/z* of an ion, in ppm); RT: retention time. Metabolites in bold were confirmed with authentic standards.

Id	Metabolite	Formula	Class [a]	Detected *m/z*	*m/z* error (ppm)	RT (min)	KEGG ID	PubChem CID	family
1	Spermidine	$C_7H_{19}N_3$	Amines	146.1653	0.54	0.85	C00315	1102	N
2	Agmatine	$C_5H_{14}N_4$	Amines	131.1292	0.91	0.89	C00179	199	N
3	**Pipecolic acid**	$C_6H_{11}NO_2$	Amines	130.0863	0.7	1.35	C00408	849	N
4	Methyl-pipecolic acid	$C_7H_{13}NO_2$	Amines	144.1019	0.31	1.17			N
5	**Arginine**	$C_6H_{14}N_4O_2$	Amino acids	175.1190	0.20	0.95	C00062	6322	AA
6	**Asparagine**	$C_4H_8N_2O_3$	Amino acids	133.0609	0.86	1.17	C00152	6267	AA
7	**Aspartic acid**	$C_4H_7NO_4$	Amino acids	134.0449	0.69	1.09	C00049	5960	AA
8	**Glutamic acid**	$C_5H_9NO_4$	Amino acids	148.0604	-0.58	1.17	C00025	4525487	AA
9	**Glutamine**	$C_5H_{10}N_2O_3$	Amino acids	147.0764	0.09	1.08	C00064	5961	AA
10	**Histidine**	$C_6H_9N_3O_2$	Amino acids	156.0769	0.68	1.00	C00135	6274	AA
11	**Hydroxyproline**	$C_5H_9NO_3$	Amino acids	132.0656	0.70	1.27	C01157	5810	AA
12	**Isoleucine**	$C_6H_{13}NO_2$	Amino acids	132.1020	0.76	2.96	C00407	6306	AA
13	**Leucine**	$C_6H_{13}NO_2$	Amino acids	132.1020	0.76	2.76	C00123	6106	AA
14	**Lysine**	$C_6H_{14}N_2O_2$	Amino acids	147.1129	0.44	0.84	C00047	5962	AA
15	**Methionine**	$C_5H_{11}NO_2S$	Amino acids	150.0584	0.36	2.04	C00073	6137	AA
16	**Phenylalanine**	$C_9H_{11}NO_2$	Amino acids	166.0862	-0.53	4.30	C00079	6140	AA
17	**Proline**	$C_5H_9NO_2$	Amino acids	116.0708	1.69	1.23	C00148	145742	AA
18	**Threonine**	$C_4H_9NO_3$	Amino acids	120.0657	1.22	1.08	C00188	6288	AA
19	**Tryptophan**	$C_{11}H_{12}N_2O_2$	Amino acids	205.0973	0.51	4.75	C00078	6305	AA
20	**Tyrosine**	$C_9H_{11}NO_3$	Amino acids	182.0813	0.54	3.20	C00082	6057	AA
21	**Valine**	$C_5H_{11}NO_2$	Amino acids	118.0863	0.48	1.14	C00183	6287	AA
22	DHBOA-Glc-Glc	$C_{20}H_{28}NO_{14}$	Benzoxazinoids	523.1773	0.59	4.48			BZ
23	DHBOA-Glc-Rh	$C_{20}H_{28}NO_{13}$	Benzoxazinoids	490.1557	0.59	4.71			BZ
24	DHBOA_Glc	$C_{14}H_{17}NO_9$	Benzoxazinoids	344.09767	0.19	4.29		592555	BZ
25	DIMBOA	$C_9H_9NO_5$	Benzoxazinoids	212.0555	0.62	5.40	C04720	2358	BZ
26	HBOA	$C_8H_7NO_3$	Benzoxazinoids	166.0499	0.34	5.92	C15769	322636	BZ
27	HBOA-Glc	$C_{14}H_{17}NO_8$	Benzoxazinoids	328.1027	0.09	4.71		14605136	BZ
28	HMBOA-Glc	$C_{15}H_{19}NO_9$	Benzoxazinoids	358.1241	-0.61	5.06			BZ
29	HMBOA	$C_9H_9NO_4$	Benzoxazinoids	196.0605	0.42	5.42		152213	BZ
30	**Apigenin-6-C-glucoside**	$C_{21}H_{20}O_{10}$	Flavonoids	433.1129	-0.16	5.18	C01714	162350	F
31	Apigenin-O-glucoside-O-pentoside	$C_{26}H_{28}O_{14}$	Flavonoids	565.1553	0.27	5.05	C04858	5280746	F
32	Chrysoeriol	$C_{16}H_{12}O_6$	Flavonoids	301.0707	0.05	6.42	C04293	5280666	F
33	Chrysoeriol-6-C-glucoside	$C_{22}H_{22}O_{11}$	Flavonoids	463.1237	0.43	5.35	C05990	442611	F
34	Chrysoeriol-C-hexosyl-O-deoxyhexoside	$C_{28}H_{32}O_{15}$	Flavonoids	609.1817	0.50	5.24			F
35	Chrysoeriol-C-hexosyl-O-hexoside	$C_{28}H_{32}O_{16}$	Flavonoids	625.1766	0.42	5.17		72193674	F
36	Luteolin-C-hexosyl-deoxyhexoside	$C_{27}H_{30}O_{15}$	Flavonoids	595.1660	0.45	5.02			F
37	Chrysoeriol-Caffeoyl-hexosyl-hexoside	$C_{15}H_{10}O_6$	Flavonoids	287.0549	-0.40	6.05	C01514	5280445	F
38	Luteolin-C-pentosyl_C_hexoside	$C_{26}H_{28}O_{15}$	Flavonoids	581.1504	0.51	4.97		44258081	F
39	Luteolin-6-C-glucoside	$C_{21}H_{20}O_{11}$	Flavonoids	449.1080	0.30	5.00	C01750	5280459	F
40	Tricin	$C_{17}H_{14}O_7$	Flavonoids	331.0812	-0.07	6.45	C10193	5281702	F
41	Tricin-glucoside	$C_{23}H_{24}O_{12}$	Flavonoids	493.1343	0.58	5.56		5322022	F
42	Tricin 7-(6-malonylglucoside)	$C_{26}H_{26}O_{15}$	Flavonoids	579.1348	0.55	5.68		122391240	F
43	Feruloylagmatine	$C_{15}H_{22}N_4O_3$	Hydroxycinnamic acid amides	307.1765	-0.05	4.57	C18325	46173376	HC
44	Feruloylputrescine	$C_{14}H_{20}N_2O_3$	Hydroxycinnamic acid amides	265.1548	0.32	4.70	C10497	5281796	HC
45	Caffeoylputrescine	$C_{13}H_{18}N_2O_3$	Hydroxycinnamic acid amides	251.1390	0.07	4.47	C03002□	5911	HC
46	Coumaroylputrescine	$C_{13}H_{18}N_2O_2$	Hydroxycinnamic acid amides	235.1441	0.21	4.50			HC
47	Caffeoylagmatine	$C_{14}H_{20}N_4O_3$	Hydroxycinnamic acid amides	293.1608	0.06	4.52			HC
48	Sinapoylputrescine	$C_{15}H_{22}N_2O_4$	Hydroxycinnamic acid amides	295.1653	0.22	4.56			HC
49	Sinapoylagmatine	$C_{16}H_{24}N_4O_4$	Hydroxycinnamic acid amides	337.187	0.09	4.65			HC
50	Coumaroylagmatine	$C_{14}H_{20}N_4O_2$	Hydroxycinnamic acid amides	277.166	0.35	4.66	C04498	5280691	HC
51	Feruloylcadaverine	$C_{15}H_{22}N_2O_3$	Hydroxycinnamic acid amides	279.1702	0.42	4.85			HC
52	**Jasmonic acid**	$C_{12}H_{18}O_3$	Phytohormones	211.1329	0.23	6.27	C08491	5281166	H
53	**Methyl jasmonate**	$C_{13}H_{20}O_3$	Phytohormones	225.14855	0.13	7.07	C11512	13682	H

[a] Class was classified according to KEGG (Kyoto Encyclopedia of Genes and Genomes; http://www.genome.ad.jp/kegg/) and PubChem (http://pubchem.ncbi.nlm.nih.gov) databases. Id: identifier; *m/z*: mass-to-charge ratio; *m/z* error (difference between the measured *m/z* and the calculated *m/z* of an ion, represented in ppm); RT: retention time. Compounds indicated in bold were confirmed with authentic standards.

Supplemental Table 3. Non-targeted analysis of differentially accumulated ions between I and NI leaves at 48 hpi. Ions were selected based on a comparison of I and NI leaves at 48 hpi, with p-value threshold < 0.05 (two-group Welch t-test) and a fold change threshold ≥ 2. Ions were sorted by retention time (RT) in order to group ions potentially originating from the same molecule. Putative molecular formulas were proposed based on the precise mass of the ions, isotopic ratios, adducts and loss of neutrals, as well as by comparison with published literature.

Group	Identifier	fold I / NI	pvalue	m/z	RT (sec)	Molecular formula	Name / Chemical structure
NA	M214T66	16,80	4,24E-03	214,05893	66,1		
NA	M419T78	4,54	3,60E-02	419,15893	78,3	isotope	
NA	M418T79	2,93	2,45E-02	418,15552	79,1	C14 H28 O13 N	
NA	M256T116	3,28	1,61E-03	256,08156	115,8		
1	M198T130	6,84	4,55E-04	198,07616	129,5	C9 H12 O4 N	Hydroxytyrosine
NA	M151T245	4,59	1,24E-05	151,04239	245,2	C5 H11 O3 S	
NA	M304T247	2,48	3,60E-02	304,05185	247,4		
2	M251T249	5,49	3,20E-02	251,13897	248,5	C13 H19 O3 N2	Coumaroyl-hydroxyputrescine
3	M281T254	8,32	9,86E-03	281,14954	253,7	C14 H21 O4 N2	Feruloyl-hydroxyputrescine
4	M293T254	22,63	1,32E-02	293,16074	253,9	C14 H21 O3 N4	Coumaroyl-hydroxy-agmatine
4	M294T254	24,36	1,41E-02	294,16406	254,3	$C13^{13}C$ H21 O3 N4	isotope of M293T254
5	M147T255	7,96	1,35E-02	147,04400	254,9	C9 H7 O2	coumaroyl fragment of M291T255
5	M291T255	12,98	6,13E-03	291,14510	254,9	C14 H19 O3 N4	Coumaroyl-hydroxydehydro-agmatine
5	M292T255	28,09	7,35E-03	292,14835	255,3	$C13^{13}C$ H19 O3 N4	isotope of M292T255
5	M273T256	13,70	1,03E-02	273,13456	255,7	C14 H17 O2 N4	fragment of M291T255
5	M274T256	22,65	9,83E-03	274,13788	255,8	$C13^{13}C$ H17 O2 N4	isotope of M273T256
6	M266T257	2,50	9,32E-03	266,15799	257,1		isotope du M265T258
6	M265T258	2,91	3,03E-04	265,15466	258,0	C14H21O3N2	feruloylputrescine
7	M323T258	11,25	7,23E-04	323,17138	258,0	C15 H23 O4 N4	Feruloyl-hydroxy-agmatine
7	M324T258	3,05	2,83E-03	324,17467	258,5		isotope du M323T258
8	M321T259	5,20	6,32E-03	321,15574	259,1	C15 H21 O4 N4	Feruloyl-hydroxydehydro-agmatine
NA	M178T260	2,02	3,18E-05	178,05327	259,8	C6 H12 O3 N S	
NA	M346T260	2,46	4,84E-05	346,07911	259,9	isotope	
NA	M344T260	2,17	1,47E-04	344,08327	260,0	C11 H22 O7 N S2	
NA	M345T260	2,27	4,97E-04	345,08687	260,0	isotope	
NA	M144T261	4,49	2,84E-02	144,08085	261,2	C10 H10 N	
10	M307T262	6,60	1,18E-02	307,17652	261,5	C15 H23 O3 N4	Feruloylagmatine
9	M278T262	42,76	1,15E-02	278,16922	261,7	$C13^{13}C$ H21 O2 N4	isotope of Coumaroylagmatine
10	M308T265	13,91	3,27E-04	308,17977	264,5	$C14^{13}C$ H23 O3 N4	isotope of Feruloylagmatine
12	M337T266	2,83	8,24E-04	337,18705	265,7	C16 H25 O4 N4	sinapoylagmatine
11	M275T266	67,35	1,25E-02	275,15028	266,4	C14 H19 O2 N4	Coumaroyl-dehydro-agmatine
NA	M314T268	3,10	7,52E-06	314,07264	267,7	C10 H20 O6 N S2	
NA	M422T271	3,33	1,13E-02	422,15921	270,8		
NA	M227T279	2,18	2,25E-04	227,17533	279,4	C12 H23 O2 N2	
NA	M262T299	2,17	2,91E-02	262,18016	299,2		
NA	M201T299	2,21	2,79E-03	201,11215	299,5		
13	M186T301	5,27	6,12E-04	186,22169	300,9	C12 H28 N	Dodecanamine
NA	M360T302	2,94	3,28E-02	360,12892	302,1		
NA	M163T313	2,30	6,14E-03	163,13289	313,2		
NA	M363T313	8,04	2,32E-02	363,14159	313,3	C15 H19 O5 N6	
NA	M342T313	7,04	5,15E-04	342,21231	313,3	C14 H32 O8 N	
NA	M370T313	6,13	1,97E-05	370,24360	313,4	C16 H36 O8 N	
NA	M371T314	3,59	3,12E-05	371,24702	313,7		
NA	M395T317	2,34	1,95E-02	395,26402	317,2		
NA	M222T324	3,20	3,11E-03	222,07610	323,8		
NA	M143T325	3,40	1,37E-02	143,10673	324,7		
NA	M467T325	3,64	8,35E-05	467,24892	325,1		
NA	M426T330	2,38	2,21E-04	426,23350	329,9		
NA	M391T330	2,36	8,08E-05	391,19633	330,2	C18H30O9	
NA	M462T330	2,21	1,64E-02	462,11847	330,4		
NA	M409T331	2,19	7,90E-05	409,20694	331,0		
NA	M422T331	4,62	1,12E-04	422,20216	331,3		
NA	M463T334	3,27	2,12E-03	463,25397	334,1		
NA	M481T334	2,91	2,06E-03	481,26456	334,2		
NA	M482T334	4,17	6,03E-05	482,26807	334,3		
NA	M215T334	4,08	2,08E-03	215,20057	334,4	C13H27O2	
NA	M405T343	6,44	3,67E-04	405,21203	342,7		
NA	M423T343	4,10	2,01E-03	423,22260	343,4		
NA	M730T361	2,07	8,39E-03	730,34945	361,4		
NA	M742T365	2,42	8,03E-03	742,47383	365,1		
NA	M469T367	6,71	2,54E-06	469,23679	367,1		
NA	M410T376	24,37	2,55E-02	410,20214	376,2	C17 H32 O10 N	
NA	M290T377	12,07	1,95E-02	290,08695	376,6	C11 H16 O8 N	
NA	M416T377	10,48	4,36E-02	416,16087	376,7	C24 H22 O4 N3	
NA	M127T377	2,82	1,03E-03	127,03909	376,8		
NA	M429T383	4,20	3,93E-04	429,24839	383,0		
NA	M482T384	3,33	3,98E-04	482,29616	383,5		
NA	M430T384	5,27	2,44E-03	430,25176	383,5		
NA	M518T384	5,98	7,16E-03	518,18102	383,8		
NA	M411T385	3,79	1,42E-03	411,23773	384,5		
NA	M466T385	3,36	1,21E-03	466,27332	385,3		
NA	M231T387	4,27	3,17E-04	231,04993	386,5		
NA	M465T387	7,90	6,59E-04	465,27000	386,6	C18 H37 O8 N6	
NA	M396T387	2,51	1,48E-03	396,22292	386,7		
NA	M447T387	5,84	1,31E-03	447,25908	386,8	C22 H37 O8	
NA	M448T387	2,61	4,81E-03	448,26248	387,3	isotope	
NA	M143T392	2,39	3,05E-04	143,10670	391,6		
NA	M429T395	2,51	2,72E-02	429,21198	395,1	C22H35O7	
NA	M482T402	2,48	1,55E-03	482,25980	402,0		
NA	M447T403	2,08	3,93E-03	447,22256	402,6		
NA	M465T403	2,60	1,40E-03	465,23331	402,6		

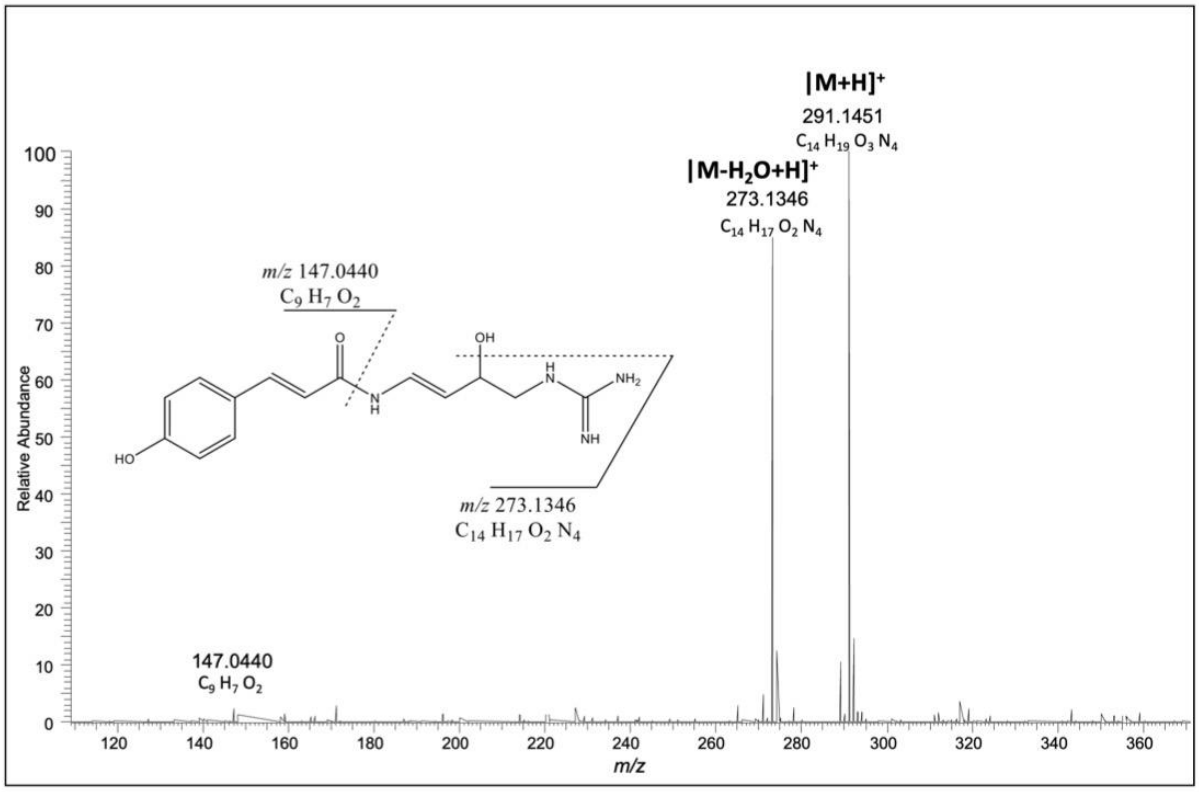

Supplemental Figure 1. Mass spectrum of the putative p-coumaroyl-3-hydroxydehydro-agmatine (M291T255). The fragmentation giving rise to the main fragments is indicated.